Available online at www.sciencedirect.com
ScienceDirect
Comput. Methods Appl. Mech. Engrg. 371 (2020) 113294
Computer methods in applied mechanics and engineering
www.elsevier.com/locate/cma

Space–time domain decomposition for two-phase flow between different rock types☆,☆☆

Elyes Ahmed[a,b,c,1], Caroline Japhet[c], Michel Kern[a,b,*]

[a] Inria, 2 rue Simone Iff, 75589 Paris, France
[b] Université Paris-Est, CERMICS (ENPC), 77455 Marne-la-Vallée, France
[c] Université Paris 13, Sorbonne Paris Cité, LAGA, CNRS (UMR 7539), 93430, Villetaneuse, France

Available online xxxx

Abstract

In Ahmed et al. (2019) a space–time domain decomposition method was proposed for two-phase flow in a porous medium composed of two different rock types, so that the capillary pressure field is discontinuous at the interface between the rocks. For this nonlinear and degenerate parabolic problem, with nonlinear and discontinuous transmission conditions on the interface, the Optimized Schwarz waveform relaxation method (OSWR) with Robin or Ventcell transmission conditions was considered. A guaranteed and fully computable a posteriori error estimate was derived, which in particular took into account the domain decomposition error.

In this paper we provide a mathematical and numerical analysis of this space–time domain decomposition method in the Robin case. Complete numerical approximation is achieved by a finite volume scheme in space and the lowest order discontinuous Galerkin method in time. We prove the existence of a weak solution of the two-phase flow subdomain problem with Robin boundary conditions by analyzing the convergence of the finite volume scheme. The domain decomposition algorithm is based on the solution of space–time nonlinear subdomain problems over the whole time interval, allowing for different time steps in different parts of the domain, adapted to the physical properties of each subdomain, and we show that such an algorithm is well-defined. Numerical experiments on three-dimensional problems with different rock types illustrate the performance of the domain decomposition method.

Keywords: Two-phase Darcy flow; Discontinuous capillary pressure; Space–time domain decomposition method; Optimized Schwarz waveform relaxation; Nonlinear and discontinuous Robin transmission conditions; Nonconforming time grids

1. Introduction

Simulations of two-phase flows through heterogeneous porous media are widely used in many applications. Among others, these models are used for gas migration around a nuclear waste repository in the subsurface [1], CO2 sequestration in saline aquifers, in petroleum engineering to predict the motion of oil in the underground, in

☆ This paper is dedicated to Professor Mary F. Wheeler on the occasion of her 80th birthday.
☆☆ This work was supported by Agence Nationale de la Recherche under grant ANR-14-CE23-0005 DEDALES.
* Corresponding author at: Inria, 2 rue Simone Iff, 75589 Paris, France.
E-mail addresses: elyes.ahmed@sintef.no (E. Ahmed), japhet@math.univ-paris13.fr (C. Japhet), Michel.Kern@inria.fr (M. Kern).
[1] Current address: SINTEF, P.O. Box 124 Blindern, 0314 Oslo, Norway.

https://doi.org/10.1016/j.cma.2020.113294
0045-7825/

the design of thermal energy storage [2], or crystal growth [3]. In such applications, the domain of calculation is a union of different rock types with different physical properties and in which the lengths of the rocks and the time scales may be highly different. Variation of the rock type means variation on the permeability but also on the relative permeability and on the capillary pressure curves, that are functions of the phase saturations. An important consequence, which is the main topic of this paper, is that the capillary pressure and the relative permeability functions may be discontinuous across the interface between different rocks. These discontinuities play a crucial role in many phenomena see e.g. [4–8]. The numerical simulation of such flows is a challenging task, and one might want to use much larger time steps for some region of the domain than for others.

In this paper a simplified two-phase flow model is considered (with one equation and no advection), see [9], to study the phenomenon of oil or gas trapping in a porous medium with several rock types.

This problem presents several theoretical and numerical difficulties: the *nonlinearity* and *degeneracy* of the parabolic equation for the saturation of one of the phases, and the *nonlinear* and *discontinuous transmission conditions* at the interface between the rocks. To our knowledge, the first existence proof for degenerate parabolic problems was given in the seminal paper [10] by showing the convergence of a semi-discrete problem in time. In this work, we follow a framework exemplified by [11,12], where the existence of weak solutions is proved through the convergence of a discrete finite volume scheme. This has recently been extended to the more general Gradient Discretization Method in [13,14]. Related results can be found in [15,16], as well as [17,18], where the nonlinearities are allowed to be only Hölder continuous. Existence results for two-phase flow problems can be found, among other works, in [19–23].

For the specific case of discontinuous capillary pressure functions, a first analysis showing that the model explains the capillary trapping phenomenon was given in [7], followed by an existence proof for a 1D model in [8] (see also [24] in the context of homogenization, and [25]). More general results for nonlinear parabolic transmission problems can be found in [26,27]. In this work we follow mostly [9] and [28] where existence results in the multi-dimensional case can be found. See also [28,29], and [30,31] for the full two-phase flow model. Several numerical schemes have been introduced in [9,32] and analyzed in [9,13,14,28,33]. In [31], the convergence of the numerical approximation of the full two–phase flow problem in a heterogeneous multidimensional porous medium is proved.

Uniqueness of a weak solution for such models is proved in [28] for a particular choice of functions characterizing the porous medium, and in [30,34] in the one-dimensional case, for the full two-phase problem with advection terms. In [31], the convergence of the numerical approximation of the full problem in a heterogeneous multidimensional porous medium is proved, without any simplification on the model or particular assumption.

Due to different hydrogeological properties of the different rocks, domain decomposition (DD) methods appear to be a natural way to solve efficiently two-phase flow models, see [35–37], and also [38–42].

This paper complements [43], where a *global-in-time* domain decomposition method for this nonlinear and degenerate parabolic problem was proposed (without analysis), using the Optimized Schwarz Waveform Relaxation algorithm (OSWR) with Robin or Ventcell transmission conditions. A guaranteed and fully computable a posteriori error estimate was derived for the finite volume — backward Euler approximation of the space–time DD algorithm, which in particular took into account the domain decomposition error and the linearization error. This enabled the design of a stopping criterion for the OSWR algorithm as well as for the linearization iterations, which together lead to important computational savings. This DD method also allows for simultaneously: (a) degenerate parabolic problems; (b) nonlinear and discontinuous transmission conditions; (c) Robin and Ventcell transmission conditions; (d) global-in-time formulation, and we are not aware of any domain decomposition algorithm proposed and analyzed in that case. Some of these ingredients have been introduced previously independently in [44–49] and the references therein. The use of optimized (Robin or Ventcell) transmission operators allows physically more valuable information to be exchanged between the subdomains and improves drastically convergence rates, see [44,45,50–54] and the references therein for linear problems, and [47,55] for problems with nonlinear reaction terms. Robin–Robin methods have also been used to improve the transmission condition in coupled problems, see for instance [56–58] for the Darcy–Stokes system, or [59–62] for ocean–atmosphere models. The use of a global-in-time DD method together with discontinuous Galerkin (DG) for the time discretization provides flexibility in using different time steps in different parts of the domain, adapted to the physical properties of each subdomain, see [45,63,64] for diffusion and advection–diffusion problems.

The two main contributions of this paper are:

- in Section 4, a proof for the *existence of a weak solution* to the two-phase flow subdomain problem with Robin boundary conditions, by analyzing the convergence of the finite volume scheme, extending the work in [9]. These results were announced in [65];
- in Section 5, a proof that the space–time DD algorithm, based on solving space–time nonlinear Robin subdomain problems, with local time stepping, is well-defined.

In Section 2 we recall the physical model and define a multidomain weak solution. Then, in Section 3, we recall, in the Robin case, the space–time DD method introduced in [43], and give the associated interface problem. In Section 4, after introducing the discrete Robin problem in a subdomain based on a finite volume scheme and the lowest order DG method for the time discretization, we prove the existence of a weak solution of the two-phase flow subdomain problem with Robin boundary conditions, by analyzing the convergence of the finite volume scheme. Some of the details of the proof were omitted for lack of space and can be found in [66]. Then, in Section 5 we show that our discrete space–time DD algorithm is well-defined. The method is numerically validated on several examples in three space dimensions in Section 6.

2. Presentation of the problem

Most of the content of this section, with the important exception of the definition of a weak solution, is taken from the companion paper [43], which is complementary to the present work by presenting error estimates and stopping criteria for the domain decomposition iterations. Most of this material actually goes back to [9], and has been included in order to keep the present paper self-contained.

Let Ω be an open bounded domain of $\mathbb{R}^d$, $d = 2$ or 3, which is assumed to be polygonal if $d = 2$ and polyhedral if $d = 3$. We denote by $\partial\Omega$ its boundary (supposed to be Lipschitz-continuous) and by $\mathbf{n}$ the unit normal to $\partial\Omega$, outward to Ω. Let a time interval $(0, T)$ be given with $T > 0$. We consider a simplified model of a two-phase flow through a heterogeneous porous medium, in which the advection is neglected. Assuming that there are only two phases occupying the porous medium Ω, say gas and water, and that each phase is composed of a single component, the mathematical form of this problem as it is presented in [9,28] is as follows: given initial and boundary gas saturations u_0 and g, as well as a source term f, find $u : \Omega \times [0, T] \to [0, 1]$ such that

$$\partial_t u - \nabla \cdot (\lambda(u, \mathbf{x})\nabla\pi(u, \mathbf{x})) = f, \quad \text{in } \Omega \times (0, T), \tag{2.1a}$$

$$u(\cdot, 0) = u_0, \quad \text{in } \Omega, \tag{2.1b}$$

$$u = g, \quad \text{on } \partial\Omega \times (0, T). \tag{2.1c}$$

Here u is the *gas saturation* (and therefore $(1-u)$ is the water saturation), $\pi(u, \mathbf{x}) : [0, 1] \times \Omega \to \mathbb{R}$ is the *capillary pressure*, and $\lambda(u, \mathbf{x}) : [0, 1] \times \Omega \to \mathbb{R}$ is the *global mobility* of the gas. One can refer to [9,19,67] for a derivation of (2.1) from the complete two-phase flow model.

Model (2.1) differs from the full two–phase flow model in two important aspects: first, it involves only a scalar equation, whereas the two-phase flow model has two equations (usually one equation for the pressure of one phase, and one equation for the saturation of the other phase, though other choices are possible), and second, the equation is parabolic, while two–phase flow models have a significant hyperbolic component. Both simplifications were made in order to follow the set-up of [9], and because this paper is the first application of the OSWR method to this type of problems. We emphasize that both restrictions can be lifted: the multidomain coupled problem (without domain decomposition) has been treated in [31], while the OSWR method has been extended to the diffusion–advection case in [64], See also [37] for related work, and [41] for a different domain decomposition method applied to the full two–phase flow model.

For simplicity, we consider only Dirichlet boundary conditions on $\partial\Omega$. Other types of boundary conditions could be dealt with the same way as in [9,28,68]. The model problem given by (2.1a) is a nonlinear degenerate parabolic problem as the global mobility $\lambda(u) \to 0$ for $u \to 0$ and 1, and, moreover, $\pi'(u) \to 0$ for $u \to 0$ (see [19,69]). This situation corresponds to the "slow diffusion" case [17,70].

2.1. Flow between two rock types

In this part, we particularize the model problem (2.1a) to a porous medium with different capillary pressure curves π_i in each subdomain, following [9]. For simplicity we suppose that Ω is composed of two non-overlapping subdomains Ω_i, $i = 1, 2$, which are both open polygonal subsets of $\mathbb{R}^d$ with Lipschitz-continuous boundary. However, the analysis given below can be generalized to the case of multiple subdomains (see Section 6).

We denote by Γ the interface between Ω_1 and Ω_2, i.e., $\Gamma = (\partial\Omega_1 \cap \partial\Omega_2)^\circ$. Let $\Gamma_i^{\mathrm{D}} = \partial\Omega_i \cap \partial\Omega$. Both data λ and π, which can in general depend on the physical characteristics of the rock, are henceforth supposed to be homogeneous in each subdomain Ω_i, $i = 1, 2$, i.e., $\lambda_i(\cdot) := \lambda_{|\Omega_i}(\cdot) = \lambda(\cdot, \mathbf{x}), \forall \mathbf{x} \in \Omega_i$, and similarly for π_i. The Eqs. (2.1a) in *each subdomain* Ω_i then read as

$$\partial_t u_i - \nabla \cdot (\lambda_i(u_i)\nabla\pi_i(u_i)) = f_i, \quad \text{in } \Omega_i \times (0, T), \tag{2.2a}$$

$$u_i(\cdot, 0) = u_0, \quad \text{in } \Omega_i, \tag{2.2b}$$

$$u_i = g_i, \quad \text{on } \Gamma_i^{\mathrm{D}} \times (0, T). \tag{2.2c}$$

We use the notation $v_i = v|_{\Omega_i}$ for an arbitrary function v.

Before transcribing the transmission conditions on the interface Γ, we make precise the assumptions on the data (further generalizations are possible, bringing more technicalities):

Assumption 2.1 (*Data*)**.**

1. For $i \in \{1, 2\}$, $\pi_i \in C^1([0, 1], \mathbb{R})$ can be extended in a continuous way to a function (still denoted by π_i) such that $\pi_i(u) = \pi_i(0)$ for all $u \leq 0$ and $\pi_i(u) = \pi_i(1)$ for all $u \geq 1$. Moreover, $\pi_i|_{[0,1]}$ is a strictly increasing function. Following [9], we also assume that $\pi_1(0) \leq \pi_2(0) < \pi_1(1) \leq \pi_2(1)$.
2. For $i \in \{1, 2\}$, $\lambda_i \in C^0([0, 1], \mathbb{R}^+)$ is bounded and can be extended in a continuous way to a function (still denoted by λ_i) such that $\lambda_i(u) = \lambda_i(0)$ for all $u \leq 0$ and $\lambda_i(u) = \lambda_i(1)$ for all $u \geq 1$. We denote by C_λ an upper bound of $\lambda_i(u)$, $u \in \mathbb{R}$.
3. The initial condition is such that $u_0 \in L^\infty(\Omega)$ with $0 \leq u_0 \leq 1$ a.e. in Ω.
4. The boundary conditions $0 \leq g_i \leq 1$ are traces of some functions from $L^2(0, T; H^1(\Omega_i))$.
5. The source term is such that $f \in L^2(0, T; L^2(\Omega))$. For simplicity we further assume that f is piecewise constant in time with respect to the temporal mesh introduced in Section 4.1.2.

Remark 2.1. Some comments on Assumption 2.1 may be helpful:

- Assumption 1 above is somewhat restrictive, as it excludes physically relevant situations. For example, it does not cover the case of the commonly used Brooks–Corey saturation model [71]. The restriction to Lipschitz continuous capillary pressure function is made for theoretical reasons. In Section 6, among the numerical examples that are shown, some satisfy the assumptions above, and some do not, even though the method still behaves well.
- Similar degenerate parabolic problems have been studied under the more general assumption that the capillary pressure is only Hölder continuous (see [18] and references therein).
- It is natural to assume that the boundary conditions g_i match where the interface Γ meets the boundary. in the sense that $\pi_1(g_1(\mathbf{x})) = \pi_2(g_2(\mathbf{x}))$ for all $\mathbf{x} \in \Gamma \cap \Gamma_1^{\mathrm{D}}$ and all $\mathbf{x} \in \Gamma \cap \Gamma_2^{\mathrm{D}}$. However this is not necessary to define weak solutions.

We give now the *transmission conditions* needed to connect the subdomain problems (2.2), for $i = 1, 2$. We consider the general case where the capillarity pressure curves may be *non-matching*: $\pi_1(0) \neq \pi_2(0)$ or $\pi_1(1) \neq \pi_2(1)$. Consequently, not only the saturation is discontinuous at the medium interface, but also the capillary pressure field. The transmission conditions have been studied in [7,9,19,32], see also [8,24,31,34]. They have direct consequences on the behavior of the capillary pressures on both sides of the interface Γ. Here we follow the discussion in [9]. Because of Assumption 2.1–1, there exist two unique real numbers $(u_1^*, u_2^*) \in [0, 1]^2$ satisfying respectively $\pi_1(u_1^*) = \pi_2(0)$ and $\pi_2(u_2^*) = \pi_1(1)$. Then, if $u_1 \geq u_1^*$ and $u_2 \leq u_2^*$, we can prescribe the connection of the capillary pressures $\pi_1(u_1) = \pi_2(u_2)$ on the interface Γ. If $0 \leq u_1 \leq u_1^*$, the model imposes $u_2 = 0$, and the gas phase is entrapped in the rock Ω_1, and the water flows across Γ. In the same way, if $u_2^* \leq u_2 \leq 1$, the model

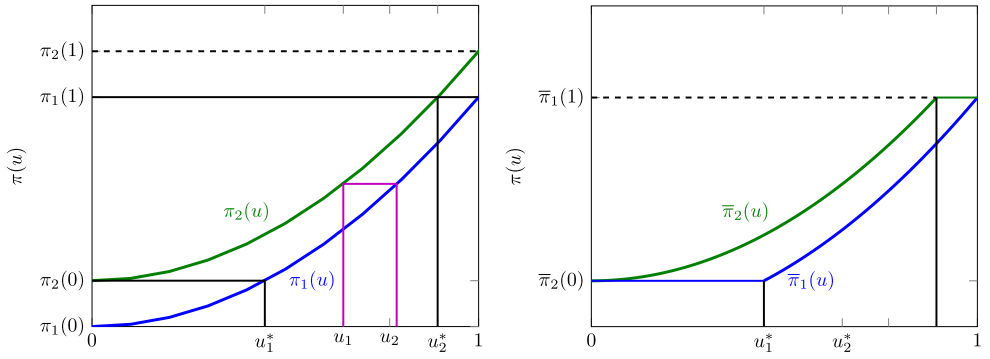

Fig. 2.1. Capillary pressure curves (left) and truncated capillary pressures curves (right).

prescribes $u_1 = 1$, and the water phase is captured in Ω_2 as a discontinuous phase, and the gas flows across Γ (see Fig. 2.1 left). Following [9], these conditions on the gas–water saturations on the interface Γ are simply given by

$$\overline{\pi}_1(u_1) = \overline{\pi}_2(u_2), \qquad \text{on } \Gamma \times (0,T), \tag{2.3a}$$

$$\lambda_1(u_1)\nabla\pi_1(u_1)\cdot\mathbf{n}_1 = -\lambda_2(u_2)\nabla\pi_2(u_2)\cdot\mathbf{n}_2, \quad \text{on } \Gamma \times (0,T), \tag{2.3b}$$

where $\overline{\pi}_i$, for $i = 1, 2$, are truncated capillary pressure functions given on $[0, 1]$ respectively by $\overline{\pi}_1 : u \mapsto \max(\pi_1(u), \pi_2(0))$ and $\overline{\pi}_2 : u \mapsto \min(\pi_2(u), \pi_1(1))$ (see Fig. 2.1 right).

If $\pi_1(0) = \pi_2(0)$ and $\pi_1(1) = \pi_2(1)$, then (2.3a) becomes $\pi_1(u_1) = \pi_2(u_2)$, on $\Gamma \times (0, T)$.

In [7], it has been established that the model problem (2.2) together with the transmission conditions (2.3) has the necessary mathematical properties to explain the phenomena of gas trapping (see also [9,34,72]).

2.2. *Transformation of the equations and weak formulation*

Still following [9], we present here the mathematical quantities and function spaces used to characterize the weak solution to the multidomain problem (2.2) with the conditions (2.3). That of the problem (2.2) with the conditions (2.3) can be deduced straightforwardly from this later, see [28]. As Ω_i is a homogeneous rock type, so that π_i and λ_i do not depend on $\mathbf{x}$, one can define the Kirchhoff transform

$$\varphi_i : \begin{cases} [0,1] & \longrightarrow & \mathbb{R}^+ \\ s & \longmapsto & \int_0^s \lambda_i(a)\pi_i'(a)\mathrm{d}a. \end{cases} \tag{2.4}$$

The function φ_i is Lipschitz-continuous and increasing on $[0, 1]$, we denote by $L_{\varphi,i}$ its Lipschitz constant and we let $L_\varphi := \max\left(L_{\varphi,1}, L_{\varphi,2}\right)$. We extend the function φ_i from $[0, 1]$ to $\mathbb{R}$ so that $\varphi_i(u) = \varphi_i(0)$ for all $u \le 0$ and $\varphi_i(u) = \varphi_i(1)$ for all $u \ge 1$.

Following [9, Lemma 1.2] (see also [28,34]), we now introduce the strictly increasing function $\phi : [\pi_2(0), \pi_1(1)] \to \mathbb{R}^+$ defined by $\phi(u) = \int_{\pi_2(0)}^s \min_{j\in\{1,2\}}(\lambda_j \circ \pi_j^{-1}(a))\,\mathrm{d}a$, and we let $\Pi_i := \phi \circ \overline{\pi}_i$, for $i \in \{1, 2\}$. The functions $\Pi_i|_{[0,1]}$ are differentiable and increasing. We let $\Pi_i(u) = \Pi_i(0)$ for all $u \le 0$ and $\Pi_i(u) = \Pi_i(1)$ for all $u \ge 1$ and define the function Π by

$$\Pi(u, \mathbf{x}) = \Pi_i(u), \quad \text{for } \mathbf{x} \in \Omega_i.$$

The functions Π_i are more regular than $\overline{\pi}_i$, which allows to connect Π_1 and Π_2 instead of $\overline{\pi}_1$ and $\overline{\pi}_2$, that is, for all $(u_1, u_2) \in \mathbb{R}^2$, we have the crucial *equivalence property*

$$\overline{\pi}_1(u_1) = \overline{\pi}_2(u_2) \Leftrightarrow \Pi_1(u_1) = \Pi_2(u_2).$$

Finally, it is shown in [9, Lemma 1.2] that, under Assumption 2.1, the function $\beta_i := \Pi_i \circ \varphi_i^{-1}$ is Lipschitz-continuous with a Lipschitz constant lower than 1:

$$|\Pi_i(a) - \Pi_i(b)| \le |\varphi_i(a) - \varphi_i(b)|, \quad \forall (a, b) \in [0, 1]^2. \tag{2.5}$$

We now apply the Kirchhoff transformation (2.4) separately in each subdomain, giving an equivalent formulation suitable for *mathematical analysis*: find u_i such that

$$\partial_t u_i - \Delta\varphi_i(u_i) = f_i, \qquad \text{in } \Omega_i \times (0,T), \tag{2.6a}$$
$$u_i(\cdot,0) = u_0, \qquad \text{in } \Omega_i, \tag{2.6b}$$
$$\varphi_i(u_i) = \varphi_i(g_i), \quad \text{on } \Gamma_i^{\mathrm{D}} \times (0,T), \tag{2.6c}$$

together with the conditions at the interface relying on the smoother functions Π_i

$$\Pi_1(u_1) = \Pi_2(u_2), \qquad \text{on } \Gamma \times (0,T), \tag{2.7a}$$
$$\nabla\varphi_1(u_1)\cdot\mathbf{n}_1 = -\nabla\varphi_2(u_2)\cdot\mathbf{n}_2, \quad \text{on } \Gamma \times (0,T). \tag{2.7b}$$

Now, we define a weak solution to problem (2.6a) to (2.7b). We introduce the notation

$$H^1_{\varphi_i(g_i)}(\Omega_i) := \{v \in H^1(\Omega_i),\, v = \varphi_i(g_i) \text{ on } \Gamma_i^{\mathrm{D}}\}$$
$$H^1_{\Pi(g,\cdot)} := \{v \in H^1(\Omega),\, v = \Pi(g,\cdot) \text{ on } \partial\Omega\},$$
$$\tilde{X} := \left\{\psi \in H^1(\Omega\times(0,T)),\ \psi = 0 \text{ on } \partial\Omega,\ \psi(.,T) = 0\right\}.$$

Definition 2.1 (*Multidomain Weak Solution*)**.** A function u is said to be a weak solution to problem (2.6a) to (2.7b) if it satisfies:

1. $u \in L^\infty(\Omega\times(0,T))$, $0 \le u(\mathbf{x},t) \le 1\, a.e.$ in $\Omega\times(0,T)$,
2. $\varphi_i(u_i) \in L^2(0,T; H^1_{\varphi_i(g_i)})$, $i \in \{1,2\}$,
3. $\Pi(u,\cdot) \in L^2(0,T, H^1_{\Pi(g,\cdot)}(\Omega))$,
4. For all $\psi \in \tilde{X}$, the following integral equality holds:

$$\sum_{i=1}^{2}\int_{\Omega_i}\int_0^T u_i(\mathbf{x},t)\partial_t\psi(\mathbf{x},t)\,\mathrm{d}\mathbf{x}\mathrm{d}t + \sum_{i=1}^{2}\int_{\Omega_i} u_0(\mathbf{x})\psi(\mathbf{x},0)\,\mathrm{d}\mathbf{x} - \sum_{i=1}^{2}\int_{\Omega_i}\int_0^T \nabla\varphi_i(u_i(\mathbf{x},t))\cdot\nabla\psi(\mathbf{x},t)\,\mathrm{d}\mathbf{x}\mathrm{d}t = 0.$$

For a sufficiently regular weak solution u, the continuity of the flux condition, namely $[\nabla\varphi(u)\cdot\mathbf{n}] = 0$ on Γ, is fulfilled by point 4 of the definition while the condition $[\Pi(u)] = 0$ on Γ is imposed in space using point 3. In fact, using point 2 together with the fact that $\Pi\circ\varphi^{-1}$ is a Lipschitz continuous function ensures that $\Pi_i(u_i)$ is in $L^2(0,T,H^1(\Omega_i))$, for $i \in \{1,2\}$, hence the connection of the traces on $\Gamma\times(0,T)$.

Note that the notion of weak solution used in the present paper is different than the one used in [43]. The definition used here is the same as in [9], where the existence of a weak solution in the sense of Definition 2.1 was proved under Assumption 2.1 (for Neumann boundary conditions) using the convergence of a finite volume scheme. Closely related existence result have been proved in [15, Thm. 20], [13, Thm 4.4], see also [24]. Another approach to nonlinear parabolic problems with nonlinear transmission conditions can be found in [26,27]. A more general notion of weak solution (in particular relaxing the inequalities in Assumption 2.1–1) is introduced in [34], see in particular Remark 2.4 in that paper.

For the case of matching capillary pressure curves, i.e. $\pi_1(0) = \pi_2(0)$ and $\pi_1(1) = \pi_2(1)$, uniqueness is obtained in [28]. For the more general case, uniqueness has been obtained under more restrictive assumptions, see [8,16,30,34].

3. Space–time domain decomposition method

In this section, we present a non-overlapping space–time domain decomposition to solve problem (2.6)–(2.7). More precisely, an equivalent formulation to the model problem (2.6)–(2.7) can be obtained by solving, for $i = 1, 2$, Eqs. (2.6) together with optimized Robin transmission conditions on $\Gamma\times(0,T)$

$$\begin{aligned}\nabla\varphi_1(u_1)\cdot\mathbf{n}_1 + \alpha_{12}\Pi_1(u_1) &= -\nabla\varphi_2(u_2)\cdot\mathbf{n}_2 + \alpha_{12}\Pi_2(u_2),\\ \nabla\varphi_2(u_2)\cdot\mathbf{n}_2 + \alpha_{21}\Pi_2(u_2) &= -\nabla\varphi_1(u_1)\cdot\mathbf{n}_1 + \alpha_{21}\Pi_1(u_1).\end{aligned} \qquad \text{on } \Gamma\times(0,T), \tag{3.1}$$

where α_{ij} are positive constants that can be optimized to improve the convergence factor of the algorithm, when the resulting multidomain problem is solved iteratively, see Section 3.2. This equivalence of problems (2.6)–(2.7) and (2.6)–(3.1) implies that a weak solution to the latter problem exists, and is unique under the same assumptions (see [28] for more details).

3.1. A space–time interface problem

An interface operator can be used to reformulate the multidomain problem (2.6)–(3.1) as an equivalent *interface problem*, where the unknowns are located only on the interface $\Gamma \times (0,T)$, see e.g. [73]. This formulation is based on [45], and one can generalize it as in [74,75] for the case of multiple subdomains.

For $i = 1, 2$, $j = 3 - i$, we introduce Robin to Robin operators for subdomain Ω_i as follows:

$$\begin{array}{rccl} \mathcal{S}_i : & L^2(\Gamma \times (0,T)) & \to & L^2(\Gamma \times (0,T)) \\ & \xi_i & \to & -\xi_i + (\alpha_{ij} + \alpha_{ji})\Pi_j(u_j) \end{array} \tag{3.2}$$

where u_i is the solution of the subdomain problem with Robin boundary data ξ_i:

$$\begin{aligned} \partial_t u_i - \Delta\varphi_i(u_i) &= 0, && \text{in } \Omega_i \times (0,T), \\ u_i(\cdot,0) &= u_0, && \text{in } \Omega_i, \\ \varphi_i(u_i) &= g_i && \text{on } \Gamma_i^{\mathrm{D}} \times (0,T), \\ \nabla\varphi_i(u_i)\cdot \mathbf{n}_i + \alpha_{ij}\Pi_i(u_i) &= \xi_i && \text{on } \Gamma \times (0,T). \end{aligned} \tag{3.3}$$

The (non-linear) operator $\mathcal{S}_i$ maps the Robin boundary to the new Robin data that will be transmitted to the neighboring subdomain. Note that, similarly to what was done in [74, Remark 3.1], we have eliminated the normal derivative by making use of the boundary condition, so that the transmitted quantity is actually equal to $-\nabla\varphi_i(u_i)\cdot\mathbf{n}_i + \alpha_{ji}\pi(u_i)$. This makes $\mathcal{S}_i$ well defined on $L^2(\Gamma \times (0,T))$. The same technique can be used at the discrete level to avoid computing the normal derivative numerically.

Then, the multidomain problem (2.6)–(3.1) is equivalent to the following interface problem for the two unknowns $(\xi_1, \xi_2) \in L^2(\Gamma \times (0,T))^2$:

$$\begin{aligned} \xi_1 &= \mathcal{S}_2(\xi_2), \\ \xi_2 &= \mathcal{S}_1(\xi_1), \end{aligned} \qquad \text{on } \Gamma \times (0,T). \tag{3.4}$$

This problem is nonlinear and can be solved using Newton or fixed point iterations.

3.2. The optimized Schwarz waveform relaxation algorithm

A fixed point iteration for solving the nonlinear interface problem (3.4) takes the form

$$\begin{aligned} \xi_1^k &= \mathcal{S}_2(\xi_2^{k-1}), \\ \xi_2^k &= \mathcal{S}_1(\xi_1^{k-1}), \end{aligned} \qquad \text{on } \Gamma \times (0,T). \tag{3.5}$$

This requires the solution, at every iteration $k \geq 1$, of the nonlinear subdomain problem (3.3) in Ω_i, for $i \in \{1,2\}$, to compute the action of the nonlinear operators $\mathcal{S}_1$ and $\mathcal{S}_2$ on ξ_1 and ξ_2, respectively. This fixed-point algorithm is in fact equivalent to the Optimized Schwarz Waveform Relaxation (OSWR) iterative method, introduced in [52,76] for linear problems, in [47,55] for problems with nonlinear reaction terms, and proposed in [43] for problem (2.1). This method can be written as follows:

Given an initial iterate $(\xi_i^0)_{i=1,2} \in L^2(\Gamma \times (0,T))^2$, at iteration $k \geq 1$, we solve in each subdomain $i = 1, 2$, the problem, with $j = 3 - i$,

$$\begin{aligned} \partial_t u_i^k - \Delta\varphi_i(u_i^k) &= 0, && \text{in } \Omega_i \times (0,T), \\ u_i^k(\cdot,0) &= u_0, && \text{in } \Omega_i, \\ \varphi_i(u_i^k) &= g_i && \text{on } \Gamma_i^{\mathrm{D}} \times (0,T), \\ \nabla\varphi_i(u_i^k)\cdot \mathbf{n}_i + \alpha_{ij}\Pi_i(u_i^k) &= \xi_i^{k-1} && \text{on } \Gamma \times (0,T), \end{aligned} \tag{3.6}$$

with

$$\xi_i^{k-1} := -\nabla\varphi_j(u_j^{k-1})\cdot\mathbf{n}_j + \alpha_{ij}\Pi_j(u_j^{k-1}), \quad j = 3 - i,\ k \geq 2. \tag{3.7}$$

Note that the last equation of (3.6) gives a definition of the normal derivative on the space–time interface, e.g. for subdomain Ω_j at step $k-1$, we have:

$$-\nabla\varphi_j(u_j^{k-1})\cdot\mathbf{n}_j = -\xi_j^{k-2} + \alpha_{ji}\Pi_j(u_j^{k-1}). \tag{3.8}$$

Replacing (3.8) in (3.7), and shifting the iteration index by 1, we obtain an expression for the new update ξ_i^k that avoids the calculation of the normal derivative:

$$\xi_i^k = -\xi_j^{k-1} + (\alpha_{ij}+\alpha_{ji})\Pi_j(u_j^k),\ k\geq 1.$$

The parameters α_{ij} are chosen so as to minimize the convergence factor of the linearized problem, leading to optimized parameters for a linear diffusion problem with discontinuous coefficients similar to that in [45,77,78]. More precisely, the calculation of these parameters is as follows: setting $p_i = \pi_i(u_i)$, $K_i(p_i) = \lambda_i(\pi_i^{-1}(p_i))$ and $\theta_i(p_i) = \pi_i^{-1}(p_i)$, the multidomain formulation (2.2)–(2.4) also reads

$$\begin{aligned} \partial_t(\theta_i(p_i)) - \nabla\cdot(K_i(p_i)\nabla p_i) &= 0, && \text{in } \Omega_i\times(0,T),\\ p_1 &= p_2, && \text{on } \Gamma\times(0,T),\\ K_1(p_1)\nabla p_1\cdot\mathbf{n}_1 &= -K_2(p_2)\nabla p_2\cdot\mathbf{n}_2, && \text{on } \Gamma\times(0,T). \end{aligned} \tag{3.9}$$

Then the calculation of the optimized parameters is done beforehand the OSWR algorithm: we consider a linearized, frozen coefficients, version of the above problem, and calculate the parameters that minimize the convergence factor of the OSWR method applied to this linearized problem. More precisely, we approximate $\theta_i(p_i)$ by a linear function, and $K_i(p_i)$ by a constant value (e.g. the maximum value of $K_i(p_i)$). Then the optimized parameters are obtained following the methodology initiated in [51,53] for domain decomposition in space, in [44,45,52,54,76,79,80] for space–time domain decomposition, and in [55] for semilinear problems. In particular, the convergence factor of the OSWR algorithm can be computed explicitly using Fourier transform, and then the optimized Robin parameters are derived by (numerically) minimizing the L^∞-norm of the convergence factor.

The well-posedness of the subdomain problem (3.3) is proved in the next section, and in Section 5 the well-posedness of the discrete counterpart of the OSWR algorithm (3.5) is established, for conforming or non-conforming time discretization.

The convergence of the OSWR algorithm has been well studied for linear problems (see for instance [45,63]). Few results exist for non-linear problems. An example for a semilinear problem is given in [55].

4. Nonlinear Robin boundary problem: existence using a finite volume discretization

In each subdomain Ω_i, $i=1,2$, an initial boundary value problem similar to (3.3), with nonlinear Robin boundary conditions must be solved. In this section, we prove that this problem has at least one solution (we do not study uniqueness, which requires more difficult methods). In this part the index i is not necessary, we change notation temporarily and consider a Robin problem in a domain $\mathcal{O}\times(0,T)$.

We thus consider a bounded domain $\mathcal{O}\subset\mathbb{R}^d$ with polygonal boundary. For simplicity, we assume that the Robin boundary condition is given over the whole boundary $\Gamma=\partial\mathcal{O}$, but the results can easily be extended to consider mixed boundary conditions. Given a parameter $\alpha>0$ and Robin boundary data $\xi(\mathbf{x},t)$ on $\Gamma\times(0,T)$, we consider the following problem: find u defined on $\mathcal{O}\times(0,T)$ such that

$$\begin{aligned} \partial_t u - \Delta\varphi(u) &= 0, && \text{in } \mathcal{O}\times(0,T),\\ \nabla\varphi(u)\cdot\mathbf{n} + \alpha\Pi(u) &= \xi(\mathbf{x},t), && \text{on } \Gamma\times(0,T),\\ u(x,0) &= 0, && \text{in } \mathcal{O}. \end{aligned} \tag{4.1}$$

Because the functions φ and Π that define the problem were not the primary data of the original problem, we recall the hypotheses on the data of the subdomain problem (4.1) as they will be used in the current setting.

Assumption 4.1 (*Assumption on the Data*)**.**

1. The function φ is Lipschitz continuous and (strictly) increasing on $[0,1]$, the function Π is differentiable and increasing on $[0,1]$. Moreover, the function β defined implicitly by $\Pi=\beta\circ\varphi$ is assumed to be Lipschitz continuous with a Lipschitz constant less than 1 (cf. (2.5)).
2. The initial data u_0 is such that $u_0\in L^\infty(\mathcal{O})$ with $0\leq u(\mathbf{x})\leq 1$ a.e. in $\mathcal{O}$.

3. The Robin boundary data ξ is such that $\xi \in L^2(0,T;L^2(\Gamma))$ and the Robin parameter $\alpha > 0$ is chosen such that the following inequality is satisfied:

$$0 < \xi(\mathbf{x},t) < \alpha\Pi(1), \text{ a.e. } (\mathbf{x},t) \text{ in } \Gamma \times (0,T).$$

Remark 4.1. Assumption 4.1–Item 3 says that α should be chosen large enough. In the context of the OSWR algorithm, this is not a restrictive assumption. Indeed, in practice the Robin data ξ will be bounded, and a heuristic analysis for the discretization of related problems has shown that the optimized Robin parameter depends on the mesh size h like $1/h^a$ for some power $a > 0$ (see [53] and references therein for examples).

In a first step, we define a weak solution of problem (4.1), then we propose and analyze a finite volume scheme for its approximation. The finite volume scheme will be shown to converge, and any limit will be a weak solution as in Definition 4.1.

Definition 4.1 (*Weak Solution for the Local Robin Problem*)**.** A function u is said to be a weak solution to problem (4.1) if it satisfies:

1. $u \in L^\infty(\mathcal{O}\times(0,T)), \quad 0 \le u(\mathbf{x},t) \le 1$ a.e. in $\mathcal{O}\times(0,T)$,
2. $\varphi(u) \in L^2(0,T;H^1(\mathcal{O}))$,
3. For all $\psi \in \tilde{X} \underset{\text{def}}{=} \{h \in H^1(\mathcal{O}\times(0,T)),\ h(.,T)=0\}$,

$$\begin{aligned} &-\int_0^T\int_{\mathcal{O}} u(\mathbf{x},t)\partial_t\psi(\mathbf{x},t)\,\mathrm{d}\mathbf{x}\mathrm{d}t - \int_{\mathcal{O}} u_0\psi(\mathbf{x},0)\,\mathrm{d}\mathbf{x} \\ &+\int_0^T\int_{\mathcal{O}} \nabla\varphi(u(\mathbf{x},t))\cdot\nabla\psi(\mathbf{x},t)\,\mathrm{d}\mathbf{x}\mathrm{d}t + \alpha\int_0^T\int_{\Gamma}\Pi(u(\mathbf{x},t))\psi\,\mathrm{d}\gamma(\mathbf{x})\mathrm{d}t \\ &=\int_0^T\int_{\Gamma}\xi(\mathbf{x},t)\psi\,\mathrm{d}\gamma(\mathbf{x})\mathrm{d}t, \end{aligned} \tag{4.2}$$

where $\mathrm{d}\gamma(\mathbf{x})$ is the $(d-1)$-dimensional Lebesgue measure on $\partial\mathcal{O}$.

Remark 4.2. Because of Assumption 4.1–Item 1, the fact that $\varphi(u) \in L^2(0,T,H^1(\mathcal{O}))$ automatically implies that $\Pi(u) \in L^2(0,T,H^1(\mathcal{O}))$, so that $\Pi(u)$ has a trace on the boundary Γ and the last integral on the left-hand side of (4.2) is well defined.

Theorem 4.1. *Under Assumption 4.1, there exists a weak solution to problem (4.1) in the sense of Definition 4.1.*

The proof of Theorem 4.1 will be carried out in the rest of this section, through the study of an approximate solution defined by a finite volume method. Precisely, we prove that, if we discretize problem (4.1) using a first order finite volume scheme (see [11,12]), then the scheme admits a unique solution (cf. Proposition 4.2) that converges to a weak solution in the sense of Definition 4.1 (cf. Theorem 4.2).

4.1. A space–time fully discrete approximation scheme based on finite volume in space and discontinuous Galerkin in time

We introduce here partitions of $\mathcal{O}$ and Γ, time discretization, and discrete function spaces.

4.1.1. Partitions of $\mathcal{O}$ and Γ

Let $\mathcal{T}_h$ be a partition of the subdomain $\mathcal{O}$ into elements K, such that $\overline{\mathcal{O}} = \cup_{K\in\mathcal{T}_h} K$; here we suppose that the elements are either simplices or rectangular parallelepipeds but general elements can be treated via sub-meshes, see [81] and the references therein. Moreover, we assume that the partition is conforming in the sense that if K, $L \in \mathcal{T}_h$, $K \neq L$, then $K \cap L$ is either an empty set, a common face, edge, or vertex of K and L.

We denote by $\mathcal{F}_h$ the set of all the faces of $\mathcal{T}_h$. The interior mesh faces in $\mathcal{T}_h$ are collected into the set $\mathcal{F}_h^{\text{int}}$, whereas the faces of $\mathcal{T}_h$ lying on Γ are collected in the set $\mathcal{F}_h^{\Gamma}$. For an element $K \in \mathcal{T}_h$, we denote by $\mathcal{N}(K)$ the set of its neighbors. The notation $\mathcal{F}_K$ stands for all the faces of an element $K \in \mathcal{T}_h$, and $\mathcal{F}_{K,\Gamma} = \mathcal{F}_K \cap \mathcal{F}_h^{\Gamma}$.

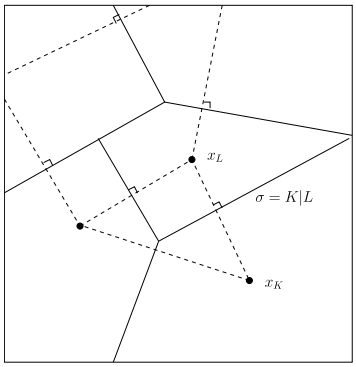

Fig. 4.1. Notation for admissible meshes in two space dimensions.

For all $K \in \mathcal{T}_h$, diam(K) denotes the diameter of K and $|K|$ its volume. The volume of a face σ is denoted by $|\sigma|$. Finally, we use the notation $\mathbf{x}_K$ to denote the "center" of the cell $K \in \mathcal{T}_h$. If $\sigma = K|L \in \mathcal{F}_h$ separates the cells K and L, $d_{K,L}$ denotes the Euclidean distance between $\mathbf{x}_K$ and $\mathbf{x}_L$, and $d_{K,\sigma}$ for $\sigma \in \mathcal{F}_K$ denotes the distance from $\mathbf{x}_K$ to σ. For $\sigma \in \mathcal{F}_K$, we denote by $\tau_{K,\sigma}$ the transmissivity of K through σ, given by $\tau_{K,\sigma} = \frac{|\sigma|}{d_{K,\sigma}}$. If $\sigma = K|L$, we use $\tau_{K,L} = \frac{|\sigma|}{d_{K,L}}$.

We assume that the mesh $\mathcal{T}_h$ satisfies the following orthogonality condition (see [12]): for an interface $\sigma = K|L$, the line segment $\mathbf{x}_K\mathbf{x}_L$ is orthogonal to this interface (see Fig. 4.1).

The size of the mesh is defined by

$$\text{size}(\mathcal{T}) = \max_{K\in\mathcal{T}} \text{diam}(K), \tag{4.3}$$

and the regularity measure of the mesh is defined by

$$\text{reg}(\mathcal{T}) = \max_{K\in\mathcal{T}}\Big(\max_{\sigma\in\mathcal{F}_K} \frac{\text{diam}(K)}{d_{K,\sigma}}\Big). \tag{4.4}$$

4.1.2. Time discretization

For an integer $M \geq 0$, let $(\tau^n)_{0\leq n\leq M}$ denote a sequence of positive real numbers corresponding to the discrete time steps such that $T = \sum_{n=1}^{M} \tau^n$. Let $t^0 = 0$, and $t^n = \sum_{j=1}^{n} \tau^j$, $1 \leq n \leq M$, be the discrete times. We denote by $\mathcal{M}$ the partition of the time interval $(0, T)$ into sub-intervals $J^n = (t^{n-1}, t^n]$, and set $\tau^n := t^n - t^{n-1}$ for all $1 \leq n \leq M$.

4.1.3. Discrete function spaces

Given a partition $\mathcal{T}_h$ of $\mathcal{O}$ and a time discretization $\mathcal{M}$ satisfying the conditions listed in Sections 4.1.1 and 4.1.2, we say that $\mathcal{D} = (\mathcal{T}_h, \mathcal{M})$ is an *admissible space–time discretization* of $\mathcal{O} \times (0, T)$. We then denote size$(\mathcal{D})$ = max(size$(\mathcal{T}_h)$, τ) and reg$(\mathcal{D})$ = reg$(\mathcal{T}_h)$.

Definition 4.2. Let $\mathcal{D}$ be an admissible discretization of $\mathcal{O} \times (0, T)$. We denote by $\mathcal{X}(\mathcal{D})$ the functional space of piecewise constant functions $u_\mathcal{D}$ defined on $\mathcal{O} \times (0, T)$:

$$\mathcal{X}(\mathcal{D}) = \big\{u_\mathcal{D} : \mathcal{O} \times (0, T) \to \mathbb{R} \text{ s.t for all } (K, J) \in \mathcal{T} \times \mathcal{M},\ u_\mathcal{D} \text{ is constant on } K \times J\big\}. \tag{4.5}$$

Functions in $\mathcal{X}(\mathcal{D})$ have a trace on Γ, and the trace operator $\overline{\gamma}$ is defined, for $u_\mathcal{D} \in \mathcal{X}(\mathcal{D})$, by $\overline{\gamma}(u) = u_\sigma$ for $\sigma \in \mathcal{F}_h^\Gamma$. Finally, the space $\mathcal{X}(\mathcal{D})$ will be endowed with the discrete $L^2(0, T; H^1(\mathcal{O}))$-seminorm defined, for $u \in \mathcal{X}(\mathcal{D})$ by

$$|u|_{1,\mathcal{D}}^2 = \sum_{n=0}^{M} \tau^n \sum_{\sigma\in\mathcal{F}} \tau_{K,\sigma} |D_\sigma u|^2 \tag{4.6}$$

where $D_\sigma u = (u_K - u_L)$ if $\sigma \in \mathcal{F}_{int}$, $\sigma = K|L$ and $D_\sigma u = (u_K - u_\sigma)$ if $\sigma \in \mathcal{F}_{K,\Gamma}$.

We also define a norm on $\mathcal{X}(\mathcal{D})$ by

$$\|u\|_{\mathcal{D}}^2 = \sum_{0}^{N} \tau^n \|u\|_{\mathcal{T}}^2 \tag{4.7}$$

where

$$\|u\|_{\mathcal{T}}^2 = \sum_{K\in\mathcal{T}} |K||u_K|^2 + \sum_{\sigma\in\mathcal{F}} \tau_{K,\sigma}|D_\sigma u|^2 + \sum_{\sigma\in\mathcal{F}_h^\Gamma} |\sigma||u_\sigma|^2. \tag{4.8}$$

Remark 4.3. Let E be a space of functions defined on a subset G of Ω (typically a subdomain or an interface) and let $v(\cdot,t)$ be a function taking its values in E. We denote $P^0_{\mathcal{M}}(E)$ the vector space such that $v(\mathbf{x},\cdot)$, $\mathbf{x}\in G$, is piecewise constant in time:

$$P^0_{\mathcal{M}}(E) := \{v(\cdot,t) : (0,T)\to E;\ v(\cdot,t) \text{ is constant on } J^n,\ 1\le n\le M\}. \tag{4.9}$$

A function in $P^0_{\mathcal{M}}(E)$ is thus defined by the M functions $\{v^n := v(\cdot,t)|_{J^n}\}_{1\le n\le M}$ in E.

Then, functions in $\mathcal{X}(\mathcal{D})$ have a natural identification with functions in the space $P^0_{\mathcal{M}}(\mathbb{P}_0(\mathcal{F}_h))$, where $\mathbb{P}_0(\mathcal{F}_h)$ is the space of functions in $L^2(\Omega)$ piecewise constant on $\mathcal{T}_h$.

4.1.4. The fully discrete scheme

In order to obtain a finite volume discretization of problem (4.1), we integrate as usual the first equation on each cell of the mesh. The initial condition u_K^0 is given by

$$u_K^0 = \frac{1}{|K|}\int_K u_0\,\mathrm{d}\mathbf{x},\ \ \forall K\in\mathcal{T}. \tag{4.10}$$

For the following time steps we compute a discrete solution $\left(\left(u_K^{n+1}\right)_{K\in\mathcal{T}}, \left(u_\sigma^{n+1}\right)_{\sigma\in\mathcal{F}_h^\Gamma}\right)$, for all $n\in[\![0,M-1]\!]$, thanks to the scheme defined by

$$\begin{aligned} |K|\frac{u_K^{n+1}-u_K^n}{\tau^n} &+ \sum_{L\in\mathcal{N}(K)} \tau_{K,L}\left(\varphi(u_K^{n+1})-\varphi(u_L^{n+1})\right) \\ &+ \sum_{\sigma\in\mathcal{F}_{K,\Gamma}} \tau_{K,\sigma}\left(\varphi(u_K^{n+1})-\varphi(u_\sigma^{n+1})\right) = 0, \quad \forall K\in\mathcal{T}, \end{aligned} \tag{4.11}$$

$$-\tau_{K,\sigma}\left(\varphi(u_K^{n+1})-\varphi(u_\sigma^{n+1})\right) + \alpha|\sigma|\Pi(u_\sigma^{n+1}) = \xi_\sigma^{n+1}, \quad \forall\sigma\in\mathcal{F}_h^\Gamma\cap\mathcal{F}_K \tag{4.12}$$

where we set for all $\sigma\in\mathcal{F}_h^\Gamma$

$$\xi_\sigma^{n+1} = \frac{1}{\tau^n}\int_{J^n}\int_\sigma \xi(\mathbf{x},t)\,\mathrm{d}\gamma(\mathbf{x})\,\mathrm{d}t.$$

An approximate solution $u_{\mathcal{D}}\in\mathcal{X}(\mathcal{D})$ to problem (4.1) associated to the discretization $\mathcal{D}$ is defined by

$$u_{\mathcal{D}}(\mathbf{x},t) = \begin{cases} u_K^n, & \forall\mathbf{x}\in K,\ K\in\mathcal{T}, \\ u_\sigma^n, & \forall\mathbf{x}\in\sigma,\ \sigma\in\mathcal{F}_h^\Gamma, \end{cases} \qquad \forall t\in J^n, \quad n\in[\![1,M]\!] \tag{4.13}$$

where $u_{\mathcal{D}}$ is a solution of (4.10)–(4.12).

Let us emphasize that the discretization of the problem with a Robin boundary condition is performed with the help of additional unknowns that are defined on the edges of the boundary Γ. These may be eliminated when solving the resulting system (see Lemma 4.1). In most of the estimates to be presented, we shall usually keep them because they simplify the presentation of the results, with the understanding that they are functions of the interior unknowns.

4.2. Well-posedness and L^∞-stability of the scheme

This subsection is devoted to a proof that the finite volume scheme admits a unique solution that is moreover in $[0,1]^N$.

Because the proof will use Brouwer's fixed point theorem, we begin by recasting the finite volume scheme in a fixed point form. We start with a technical lemma that will allow us to eliminate the boundary unknowns whenever necessary.

Lemma 4.1. *Under Assumption 4.1–Item 3, for all $K \in \mathcal{T}$, for all $n \in [\![0, M-1]\!]$, and for all $u_K^{n+1} \in \mathbb{R}$, there exists a unique $u_\sigma^{n+1} \in [0,1]$ solution of (4.12).*

Proof. Eq. (4.12) may be rewritten as

$$\tau_{K,\sigma}\varphi(u_\sigma^{n+1}) + \alpha|\sigma|\Pi(u_\sigma^{n+1}) = \xi_\sigma^{n+1} + \tau_{K,\sigma}\varphi(u_K^{n+1}). \tag{4.14}$$

For $\alpha > 0$, the function $\theta : s \longmapsto \tau_{K,\sigma}\varphi(s) + \alpha|\sigma|\Pi(s)$ is strictly increasing on $[0,1]$, ensuring the uniqueness of the solution of (4.14). Moreover,

$$\theta(0) = 0, \quad \theta(1) = \tau_{K,\sigma}\varphi(1) + \alpha|\sigma|\Pi(1).$$

Now, using Assumption 4.1, we have $\theta(0) < \xi_\sigma^{n+1} + \tau_{K,\sigma}\varphi(u_K^{n+1}) < \theta(1)$, for any $u_K^{n+1} \in \mathbb{R}$. Existence then follows from the intermediate value theorem. □

We can now give the fixed point form of the finite volume scheme (4.11)—(4.12).

It will be convenient to temporarily denote the set of discrete unknowns at time t^n, for a fixed n, by $U^n = ((u_l)_{L\in\mathcal{T}})$. After adding and subtracting the term $\lambda_K u_K^{n+1}$ to (4.11), where λ_K is given on each cell by:

$$\lambda_K = \frac{\tau^n L_\varphi}{|K|}\Big(\sum_{L\in\mathcal{N}(K)} \tau_{K,L} + \sum_{\sigma\in\mathcal{F}_{K,\Gamma}} \tau_{K,\sigma}\Big)$$

(we justify this choice during the proof of Proposition 4.1), we see that system (4.11)–(4.12) is equivalent to

$$U^{n+1} = H(U^n, U^{n+1}) \tag{4.15}$$

where, for each $K \in \mathcal{T}$, $(H(U^n, U^{n+1}))_K = H_K(u_K^n, U^{n+1})$ is given by

$$\begin{aligned} H_K(u_K^n, U) = \frac{1}{1+\lambda_K}\Bigg(u_K^n + \lambda_K u_K + \frac{\tau^n}{|K|}\sum_{L\in\mathcal{N}(K)} \tau_{K,L}\Big(\varphi(u_L) - \varphi(u_K)\Big) \\ + \frac{\tau^n}{|K|}\sum_{\sigma\in\mathcal{F}_{K,\Gamma}} \tau_{K,\sigma}\Big(\varphi(u_{K,\sigma}) - \varphi(u_K)\Big)\Bigg), \end{aligned} \tag{4.16}$$

and we recall that $u_{K,\sigma} = \theta^{-1}(u_K)$ is a function of u_K via Lemma 4.1.

Proposition 4.1. *The following properties hold for the mapping H:*

1. *H is a non-decreasing function of each of its arguments,*
2. *H maps $[0,1]\times[0,1]^N$ to $[0,1]^N$,*

Proof. The proof is similar to that of Proposition 2.7 in [9] and is also given in detail in [66]. □

We can now state and prove an existence and uniqueness result for the scheme.

Proposition 4.2. *Let Assumptions 2.1 and 4.1 hold. Let $\mathcal{D}$ be an admissible discretization of $\mathcal{O}\times(0,T)$. There exists a discrete solution $u_\mathcal{D} \in \mathcal{X}(\mathcal{D})$ to the scheme (4.10)–(4.12) such that*

$$0 \le u_\mathcal{D} \le 1, \quad \text{almost everywhere in } \mathcal{O}\times(0,T). \tag{4.17}$$

Proof. By Lemma 4.1, we only need to prove the result for the interior unknowns. We prove the existence and the uniqueness of $\left(u_K^{n+1}\right)_{K\in\mathcal{T}}$ by induction on n. This is clear for $n = 0$, as the initial saturation $\left(u_K^0\right)_{K\in\mathcal{T}}$ is given by (4.10).

For the induction step, let us suppose now that for some $n \in \mathcal{M}$, the set $\left(u_K^n\right)_{K\in\mathcal{T}} \in [0,1]^N$ is known, and we need to prove the existence and the uniqueness of $\left(u_K^{n+1}\right)_{K\in\mathcal{T}}$ as solution of the fixed-point equation (4.15).

Existence: This follows from a straightforward application of Brouwer's fixed point theorem (see [82, thm 9.9.2] or [83, thm 6.3.2]). Indeed, by Proposition 4.1, and since u_K^n is in $[0,1]$ for all $K \in \mathcal{T}$, H maps the compact and convex set $[0,1]^N$ to itself, and is obviously continuous, hence admits a fixed point in the same set, as stated in (4.17).

Uniqueness: The proof follows exactly that in [9, Proposition 2.8], and uses the monotonicity of the mapping H. □

4.3. Convergence analysis of the scheme

The aim of this subsection is to prove that the solution of the finite volume scheme defined in the previous section converges to a limit that is a weak solution of problem (4.1)

Theorem 4.2. *Let Assumptions 2.1 and 4.1 hold. Let $(\mathcal{D}_m)_m$ be a sequence of admissible discretizations of $\mathcal{O}\times(0,T)$ and denote by $u_m = u_{\mathcal{D}_m}$ the approximate solution of the finite volume scheme (4.11), (4.12). There exists $u \in L^\infty(\mathcal{O}\times(0,T))$ such that, if $\lim_{m\to\infty} \mathrm{size}(\mathcal{D}_m) = 0$, and if there exists $\zeta > 0$ such that $\mathrm{reg}(\mathcal{D}_m) \le \zeta$, then (up to a subsequence)*

$$u_m \to u \in L^p(\mathcal{O}\times(0,T)), \quad \forall p \in [1,\infty),$$

and u is a weak solution to problem (4.1) in the sense of Definition 4.1

The proof will be broken down in several steps, following a now classical strategy, see [12], and also [9,28–30]: we first prove some a priori estimates in Section 4.3.1, so as to show that the discrete solution lies in a bounded set in $L^2(0,T;H^1(\mathcal{O}))$. Then, in Section 4.3.2, we use a result from [84] to pass to the limit in the non-linear terms. Last, in Section 4.3.3, we prove that the limit is a weak solution of problem (4.1).

4.3.1. Energy estimate

We now prove the following energy estimate.

Proposition 4.3 (*Discrete $L^2(0,T;H^1(\mathcal{O}))$ Estimate*)**.** *Let $\mathcal{D}$ be an admissible discretization of the domain $\mathcal{O}\times(0,T)$. Let $u_\mathcal{D}$ be the solution given by the scheme (4.11), (4.12). There exists a constant C such that*

$$|\varphi(u_\mathcal{D})|_{1,\mathcal{D}} + \|\overline{\gamma}(\Pi(u_\mathcal{D}))\|_{L^2(\Gamma\times(0,T))} \le C, \tag{4.18}$$

where $\overline{\gamma}(u_\mathcal{D})$ stands for the trace of $u_\mathcal{D}$ on Γ as in Definition 4.2.

Proof (*cf. prop. 2.5 in [28]*)**.** Multiplying (4.11) by $\tau^n\varphi(u_K^{n+1})$ and (4.12) by $\tau^n\varphi(u_\sigma^{n+1})$ then summing over all cells, all boundary faces and all time steps gives, after a discrete integration by parts

$$\begin{aligned}
&\sum_{n=0}^{M}\Bigg[\sum_{K\in\mathcal{T}}|K|\Big(u_K^{n+1}-u_K^n\Big)\varphi(u_K^{n+1}) + \tau^n\sum_{\substack{\sigma\in\mathcal{F}_{int}\\ \sigma=K|L}}\tau_{K,L}|\varphi(u_K^{n+1})-\varphi(u_L^{n+1})|^2\\
&\quad+\tau^n\sum_{\substack{\sigma\in\mathcal{F}_h^\Gamma\\ \mathcal{F}_{K,\Gamma}\ni\sigma}}\tau_{K,\sigma}|\varphi(u_K^{n+1})-\varphi(u_\sigma^{n+1})|^2 + \tau^n\sum_{\sigma\in\mathcal{F}_h^\Gamma}\alpha|\sigma|\Pi(u_\sigma^{n+1})\varphi(u_\sigma^{n+1})\Bigg]\\
&\quad=\sum_{n=0}^{M}\tau^n\sum_{\sigma\in\mathcal{F}_\Gamma}\xi_\sigma^{n+1}\varphi(u_\sigma^{n+1}).
\end{aligned}\tag{4.19}$$

Since φ is an increasing function, the function $f: s\mapsto\int_0^s\varphi(a)\,da$ is convex, so that

$$f(u_K^n) + \varphi(u_K^{n+1})\Big(u_K^{n+1}-u_K^n\Big) \ge f(u_K^{n+1}).$$

Thus

$$\sum_{n=0}^{M}\sum_{K\in\mathcal{T}}|K|\Big(u_K^{n+1}-u_K^n\Big)\varphi(u_K^{n+1}) \geq \sum_{K\in\mathcal{T}}|K|\Big(f(u_K^{M+1})-f(u_K^0)\Big) \geq -|\mathcal{O}|\int_0^1\varphi(a)\,da. \tag{4.20}$$

Now, using (2.5) and the fact that $\varphi(0)=0$ and $\Pi(0)=0$ we obtain

$$\alpha\sum_{n=0}^{M}\tau^n\sum_{\sigma\in\mathcal{F}_\Gamma}|\sigma|\Pi(u_\sigma^{n+1})\varphi(u_\sigma^{n+1}) \geq \alpha\sum_{n=0}^{M}\tau^n\sum_{\sigma\in\mathcal{F}_\Gamma}|\sigma||\Pi(u_\sigma^{n+1})|^2.$$

Inserting this estimate together with (4.20) in (4.19), one gets (4.18) in the form

$$|\varphi(u_\mathcal{D})|_{1,\mathcal{D}}^2+\alpha\|\overline{\gamma}(\Pi(u_\mathcal{D}))\|_{L^2(\Gamma\times(0,T))}^2 \leq |\mathcal{O}|\int_0^1\varphi(a)\,da+\varphi(1)\int_0^T\int_\Gamma\xi(\mathbf{x},t)\mathrm{d}\gamma(\mathbf{x})\mathrm{d}t. \quad \square$$

4.3.2. Application of compactness results

In order to prove convergence of $\varphi(u_m)$ towards $\varphi(u)$, we want to apply the compactness results stated in [84, Theorem 3.9]. The two-point flux scheme used in this paper is the same as that in [84, Section 4], and we rely on some of the results proved there. We first check the "structural assumptions" **Ax1**, **Ax2** and **Ax3**, which depend only on the scheme. In order to save space, we refer the reader to [84], in particular Section 3.1 for the statement of the assumptions, and Section 4.4 for the verification that they are satisfied for the two-point flux scheme used in both papers.

Assumption (Ax1) This assumption says that

$$\lim_{\xi\to 0}\sup_{m\geq 1}\sup_{v_m}\frac{\|\pi_m v_m(\cdot+\xi)-\pi_m v_m\|_{L^2(\mathcal{O})}}{\|v_m\|_\mathcal{T}}=0,$$

where π_m is the natural piecewise reconstruction operator from the space of discrete unknowns operator into $L^2(\mathcal{O})$, and the norm has been defined in (4.8). The result is proved as in [84, Section 4], using the space-translation Lemma [12, Lemma 9.3].

Assumption (Ax2) This says the reconstruction commutes with non-linear functions. This is trivial here, as the scheme uses piecewise constant functions;

Assumption (Ax3) Assumption (**Ax3**) says that, for a given function $\varphi\in C_c^\infty$, a discrete gradient of the elementwise average of φ can be controlled by $\|\nabla\varphi\|_{L^\infty(\mathcal{O})}$. See [84, sec. 4.4] for details;

Assumption (At) This assumption is only needed for multi-step schemes and is always true for one-step schemes [84, Sec. 3.2].

In addition to the energy estimate proven in Proposition 4.3, we need a result on the time derivative of the discrete solution. This is proved in the following Lemma (cf [85, Lemma 4.1] or [86, Lemma 4.1]).

Lemma 4.2. *Let $\mathcal{D}$ be an admissible discretization of $\mathcal{O}\times(0,T)$. If Assumption 4.1 holds, there exists a constant C such that, for all $\psi\in C_c^\infty(\mathcal{O}\times(0,T))$, there holds:*

$$\sum_{n=0}^{M}\tau^n\sum_{K\in\mathcal{T}}|K|\frac{u_K^{n+1}-u_K^n}{\tau^n}\psi_K^{n+1}\leq C\|\nabla\psi\|_{L^\infty(\mathcal{O}\times(0,T))}, \tag{4.21}$$

where we have let $\psi_K^{N=1}=\psi(x_K,t^{n+1})$.

Proof. We proceed as in the proof of Proposition 4.3, multiplying (4.11) by $\tau^n \psi_K^{n+1}$, and summing over all elements and all time steps. This time there are no boundary terms, because ψ vanishes on the boundary of $\mathcal{O}$, and after a discrete integration by parts we obtain $A = B$ with

$$A = \sum_{n=0}^{M} \sum_{K\in\mathcal{T}} |K|(u_K^{n+1} - u_K^n)\psi_K^{n+1}, \tag{4.22}$$

$$B = \sum_{n=0}^{M} \tau^n \sum_{\substack{\sigma\in\mathcal{F}\\ \sigma=K|L}} \tau_\sigma \left(\varphi(u_K^{n+1}) - \varphi(u_L^{n+1})\right)\left(\psi_K^{n+1} - \psi_L^{n+1}\right). \tag{4.23}$$

We now bound B using the Cauchy–Schwarz inequality:

$$|B|^2 \le B_1 B_2$$

where

$$B_1 = \sum_{n=0}^{M} \tau^n \sum_{\substack{\sigma\in\mathcal{F}\\ \sigma=K|L}} \tau_\sigma \left(\varphi(u_K^{n+1}) - \varphi(u_L^{n+1})\right)^2, \text{ and } B_2 = \sum_{n=0}^{M} \tau^n \sum_{\substack{\sigma\in\mathcal{F}\\ \sigma=K|L}} \tau_\sigma (\psi_K^{n+1} - \psi_L^{n+1})^2.$$

Thanks to Proposition 4.3 we know that B_1 is bounded by a constant, while

$$B_2 \le \left(\sum_{n=0}^{M} \tau^n \sum_{\substack{\sigma\in\mathcal{F}\\ \sigma=K|L}} \tau_\sigma d_{KL}\right) \|\nabla\psi\|^2_{L^\infty(\mathcal{O}\times(0,T))}.$$

Finally

$$\sum_{n=0}^{M} \tau^n \sum_{\substack{\sigma\in\mathcal{F}\\ \sigma=K|L}} \tau_\sigma d_{KL} \le T \sum_{\substack{\sigma\in\mathcal{F}\\ \sigma=K|L}} \tau_\sigma d_{KL},$$

and the last term is bounded by a constant depending only on $\mathcal{O}$ and the space dimension. □

We are now able to use [84, Thm. 3.9], and obtain the following result

Proposition 4.4. *Up to a subsequence, $\varphi(u_m)$ converges in $L^2(\mathcal{O}\times(0,T))$ towards $\varphi(u)$. Moreover, the limit function $\varphi(u)$ is actually in $L^2(0,T;H^1(\mathcal{O}))$.*

Proof. We check the three assumptions of [84, Proposition 3.8], using $p = 2$, $q = \infty$.

(a) We proved a space–time L^∞ bound in Proposition 4.2. This gives the required $L^\infty(0,T;L^2(\mathcal{O}))$ bound.
(b) We proceed as in [84, Lemma 4.3]. By (4.18), the discrete gradient of $\varphi(u_\mathcal{D})$ is bounded in $L^2(0,T;L^2(\mathcal{O})^d)$, and [87, Lemma A.1] (adapted to the discrete setting) then shows that $\varphi(u_\mathcal{D})$ itself is bounded in $L^2(0,T;L^2(\mathcal{O}))$, and then in $L^1(0,T;L^2(\mathcal{O}))$.
(c) The weak time derivative estimate was proved in (4.21).

We can now apply [84, Thm. 3.9] to see that $\varphi(u_m)$ converges towards $\varphi(u)$ a.e. in $(0,T)\times\mathcal{O}$, and also in $L^2(0,T;L^2(\mathcal{O}))$ by (4.17) and the dominated convergence theorem.

The last assertion is a standard consequence of Assumption **Ax1**, and was proved in [9, Thm. 2.15]. □

Remark 4.4. The result stated above for φ is also true for Π.

Corollary 4.1. *Up to a subsequence, $(u_{\mathcal{D}_m})_m$ converges towards u strongly in $L^p(\mathcal{O}\times(0,T))$ for all $p\in[1,\infty)$.*

Proof. Since $(\varphi(u_m))_m$ converges in $L^2(\mathcal{O}\times(0,T))$ towards $\varphi(u)$, it converges (up to a new subsequence) almost everywhere in $\mathcal{O}\times(0,T)$. The fact that φ^{-1} is continuous, implies that $(u_m)_m$ tends to u almost everywhere. We conclude using the uniform bound on $(\varphi(u_m))_m$ stated in Proposition 4.2. □

There now remains to prove the convergence of the trace. Note that it is known that, because β is Lipschitz, $\Pi(u) = \beta(\varphi(u))$ is in $L^2(0,T;H^1(\mathcal{O}))$ (cf. [88, Cor.3.2]). Thus the trace of $\Pi(u)$ is well defined, and will be denoted by $\Pi(u)_{|\Gamma}$.

One could also add that u has a trace because φ^{-1} is continuous (cf. [31, sec. 4.2]), so that $\Pi(u)_{|\Gamma} = \Pi(u_{|\Gamma})$.

We define the trace of a discrete function $u_{\mathcal{D}} \in \mathcal{X}(\mathcal{D})$ by

$$u_{\mathcal{D}|\Gamma}(x,t) = u_\sigma^{n+1},\ x \in \sigma, t \in (t^n, t^{n+1}].$$

Proposition 4.5. *The sequence $\Pi(u_{\mathcal{D}_m|\Gamma})$ converges in $L^1(\Gamma \times (0,T))$ towards $\Pi(u_{|\Gamma})$.*

Proof. The proof follows closely that of Proposition 4.9 in [31], with $\Pi(u_{\mathcal{D}})$ playing the role of $\varphi_i(s_{\mathcal{D}})$, ans is also given in detail in [66]. □

4.3.3. Existence of a weak solution

We now have all the elements to finish the proof of Theorem 4.2. We have shown previously that u_m converges toward u as $m \to \infty$. Moreover, it has been stated in Proposition 4.5 that $(\overline{\gamma}(\Pi(u_m)))_m$ converges towards $\overline{\gamma}(\Pi(u))$ weakly in $L^2(\Gamma \times (0,T))$. It remains to verify that u satisfies the weak formulation in the sense of Definition 4.1.

Let $\psi \in \tilde{U}_{test} = \left\{h \in C^2(\overline{\mathcal{O}} \times (0,T)),\ h(.,T) = 0\right\}$ and, for $m \in \mathbb{N}$, let u_m be the solution of (4.11), (4.12) for the admissible discretization $\mathcal{D}_m$. For all $n \in [\![0, M-1]\!]$ and for all $K \in \mathcal{T}$, we multiply (4.11) by $\psi_K^n = \psi(\mathbf{x}_K, n\tau^n)$, and (4.12) by $\psi_\sigma^n = \psi(\mathbf{x}_\sigma, n\tau^n)$ then sum over cells, all faces and over $n \in \mathcal{M}$ to obtain

$$\sum_{i=1}^{4} T_{i,m} = G_m,$$

where

$$T_{1,m} = \sum_{n=0}^{M} \sum_{K\in\mathcal{T}} |K| \left(u_K^{n+1} - u_K^{n+1}\right) \psi_K^n,$$

$$T_{2,m} = \sum_{n=0}^{M} \tau^n \sum_{L\in\mathcal{N}(K)} \tau_{K,L} \left(\varphi(u_K^{n+1}) - \varphi(u_L^{n+1})\right) \psi_K^n,$$

$$T_{3,m} = \sum_{n=0}^{M} \tau^n \sum_{\sigma\in\mathcal{F}_{K,\Gamma}} \tau_{K,\sigma} \left(\varphi(u_K^{n+1}) - \varphi(u_\sigma^{n+1})\right) \left(\psi_K^n - \psi_\sigma^n\right),$$

$$T_{4,m} = \sum_{n=0}^{M} \tau^n \sum_{\sigma\in\mathcal{F}_{K,\Gamma}} \alpha|\sigma| \Pi(u_\sigma^{n+1}) \psi_\sigma^n,$$

$$G_m = \sum_{n=0}^{M} \tau^n \sum_{\sigma\in\mathcal{F}_{K,\Gamma}} \xi_\sigma^{n+1} \psi_\sigma^n.$$

We follow [12, Proof of Thm. 4.2] (see also [9] and the references therein) to obtain

$$\lim_{m\to\infty} T_{1,m} = -\int_0^T \int_{\mathcal{O}} u(\mathbf{x},t) \partial_t \psi(\mathbf{x},t)\, \mathrm{d}\mathbf{x}\mathrm{d}t - \int_{\mathcal{O}} u_0 \psi(\mathbf{x},0)\, \mathrm{d}\mathbf{x}.$$

Still following [9], summing the terms by edges in $T_{2,m}$, we obtain

$$T_{2,m} = \sum_{n=0}^{M} \tau^n \sum_{\sigma=L|K\in\mathcal{T}_{int}} \tau_{K,L} \left(\varphi(u_K^{n+1}) - \varphi(u_L^{n+1})\right) \left(\psi_K^n - \psi_L^{n+1}\right),$$

and then, one shows as in [89] that

$$\lim_{m\to\infty} T_{2,m} = \int_0^T \int_{\mathcal{O}} \nabla\varphi(u(\mathbf{x},t)) \cdot \nabla\psi(\mathbf{x},t)\, \mathrm{d}\mathbf{x}\mathrm{d}t.$$

Now, we apply the Cauchy–Schwarz inequality to $T_{3,m}$ to obtain

$$T_{3,m}^2 \leq \left(\sum_{n=0}^{M}\tau^n \sum_{\sigma\in\mathcal{F}_{K,\Gamma}} \tau_{K,\sigma}\left(\varphi(u_K^{n+1}) - \varphi(u_\sigma^{n+1})\right)^2\right) \times \left(\sum_{n=0}^{M}\tau^n \sum_{\sigma\in\mathcal{F}_{K,\Gamma}} |\sigma| \frac{\left(\psi_K^n - \psi_\sigma^n\right)^2}{d_{K,\sigma}}\right).$$

The first term in the product is bounded, because of (4.18). Let C_ψ denote the Lipschitz constant of ψ. We obtain using (4.4)

$$\sum_{n=0}^{M}\tau^n \sum_{\sigma\in\mathcal{F}_{K,\Gamma}} |\sigma| \frac{\left(\psi_K^n - \psi_\sigma^n\right)^2}{d_{K,\sigma}} \leq 4T|\Gamma|C_\psi^2 \,\mathrm{size}(\mathcal{M}).$$

Hence,

$$\lim_{m\to\infty} T_{3,m} = 0.$$

Finally, using Proposition 4.5, and thanks to the regularity of the function ψ, we obtain

$$\lim_{m\to\infty} T_{4,m} = \alpha \int_0^T \int_\Gamma \Pi(u(\mathbf{x},t))\psi \,\mathrm{d}\gamma(\mathbf{x})\mathrm{d}t.$$

Similarly,

$$\lim_{m\to\infty} G_m = \int_0^T \int_\Gamma \xi(\mathbf{x},t)\psi \,\mathrm{d}\gamma(\mathbf{x})\mathrm{d}t.$$

This ends the proof of Theorem 4.2, and together with Proposition 4.2 also proves Theorem 4.1.

Remark 4.5. It is worth noticing that uniqueness of the weak solution in the sense of Definition 4.1 could be obtained using entropy inequalities, through the method of doubling variables [11,90] (see also [30] for the case of Neumann boundary conditions). Given the length of the paper, this task will not be pursued.

5. Multidomain formulation and OSWR algorithm: discrete case

The aim of this section is to design and analyze a discrete version of the multidomain formulation (2.6)–(3.1) (or equivalently (3.4)), and of the OSWR algorithm (3.6).

This discrete algorithm involves, at each iteration, the solution of local Robin subproblems of type (4.10)–(4.12). Proposition 4.2 has shown that the discrete local problems have a unique solution, and Theorem 4.1 shows that the discrete solutions converge to a solution of the continuous problem as the mesh is refined. In this section we prove that the discrete algorithm is well-defined.

Moreover, the OSWR method is global-in-time and thus allows for the use of different time steps in different subdomains. Such a method has been analyzed, in the context of Discontinuous Galerkin (DG) for the time discretization, for linear problems in [63,91], and also [45,80,92] for porous media applications.

5.1. Notations

We extend the notation of Section 4 to the multidomain case by simply adding a subscript or a superscript denoting the subdomain index to the corresponding entity (e.g. $\mathcal{M}_i$ denotes the set of all time intervals in subdomain Ω_i). We consider local time discretizations adapted to the physical characteristics of the rock (i.e. $\mathcal{M}_1$ may be different from $\mathcal{M}_2$), see Fig. 5.2. Some more notation will be needed here.

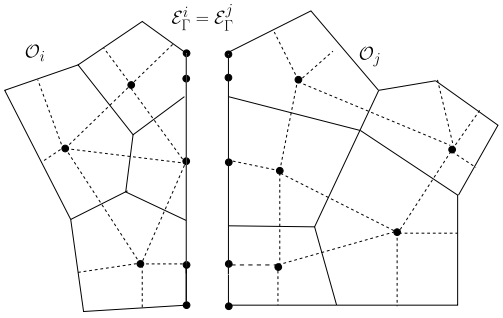

Fig. 5.1. Partition of the domain with conforming space grids.

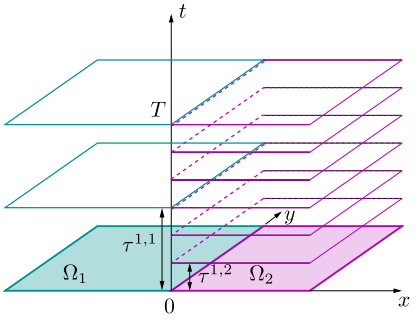

Fig. 5.2. Nonconforming time grids between two subdomains Ω_1 and Ω_2.

Admissible space–time discretization

Let $\mathcal{D}_i$ be an admissible discretization of $\Omega_i \times (0, T)$ as in Section 4.1.3. The respective spatial meshes are supposed to be matching on the interface Γ: $\mathcal{F}_{h,1}^\Gamma = \mathcal{F}_{h,2}^\Gamma$, where $\mathcal{F}_{h,i}^\Gamma$ are the faces of $\mathcal{T}_{h,i}$ lying on Γ, see Fig. 5.1.

Then, we define the admissible composite discretization associated with $\Omega \times (0, T)$.

Definition 5.1 (*Admissible Space–time Discretization of* $\Omega \times (0, T)$)**.** Let $\mathcal{D}_i$ be an admissible discretization of $\Omega_i \times (0, T)$. A composite discretization $\mathcal{D}$ of $\Omega \times (0, T)$ is given by

$$\mathcal{D} = \left(\mathcal{T}_h, \mathcal{F}_h^\Gamma, \mathcal{M}\right)$$

where $X = \cup_{i\in\{1,2\}} X_i$, for $X = \mathcal{T}_h, \mathcal{F}_h^\Gamma, \mathcal{M}$.

For subdomain Ω_i, $i = 1, 2$, let the *discrete saturation* $u_{\mathcal{D}_i} \in \mathcal{X}(\mathcal{D}_i)$ be such that, for every time step $1 \le n \le M_i$, $u_{\mathcal{D}_i}(\cdot, t^n) \in \mathbb{P}_0(\mathcal{F}_{h,i}) \times \mathbb{P}_0(\mathcal{F}_{h,i}^\Gamma)$ is identified with the vector of unknowns

$$u_{\mathcal{D}_i}(\cdot, t^n) := \left((u_K^n)_{K\in\mathcal{T}_i}, (u_\sigma^n)_{\sigma\in\mathcal{F}_\Gamma^i}\right).$$

The discrete space for the Robin data is defined, for $i = 1, 2$, as follows

$$L_{\mathcal{M}_i,h}(\Gamma) := P^0_{\mathcal{M}_i}(\mathbb{P}_0(\mathcal{F}_{h,i}^\Gamma)).$$

Time projections

For a given interface Γ, we introduce the L^2 projection operator $\mathcal{P}_{i,j}$ from $P^0_{\mathcal{M}_j}(L^2(\Gamma))$ onto $P^0_{\mathcal{M}_i}(L^2(\Gamma))$, i.e., for $\phi \in P^0_{\mathcal{M}_j}(L^2(\Gamma))$, $(\mathcal{P}_{i,j}\phi)|_{J_i^n}$ is the average value of ϕ on J_i^n, for $n \in [\![1, M_i]\!]$,

$$(\mathcal{P}_{i,j}\phi)|_{J_i^n} = \frac{1}{\tau^{n,i}} \sum_{l=1}^{M_j} \int_{J_j^l \cap J_i^n} \phi. \tag{5.1}$$

5.2. Discrete interface problem

We introduce the discrete counterpart of the subdomain solution operator $\mathcal{S}_i$, $i \in \{1,2\}$, from (3.2)–(3.3), as follows

$$\begin{aligned} \mathcal{S}_{i,h} : \; & L_{\mathcal{M}_i,h}(\Gamma) \to L_{\mathcal{M}_i,h}(\Gamma) \\ & \xi_{h\tau,i} \to -\xi_{h\tau,i} + (\alpha_{ij}+\alpha_{ji})\Pi_i(u_{\mathcal{D}_i}) \end{aligned} \tag{5.2}$$

where $u_{\mathcal{D}_i} \in \mathcal{X}(\mathcal{D}_i)$, with $u_{\mathcal{D}_i}(\cdot,t^n) := \left((u_K^n)_{K\in\mathcal{T}_i}, (u_\sigma^n)_{\sigma\in\mathcal{F}_\Gamma^i}\right)$, $n \in [\![1, M_i]\!]$, is the solution of the discrete subdomain problem with Robin boundary data $\xi_{h\tau,i}$: for $n \in [\![0, M_i-1]\!]$,

$$u_K^0 = \frac{1}{m(K)}\int_K u_0\,\mathrm{d}\mathbf{x}, \;\; \forall K \in \mathcal{T}_i, \tag{5.3a}$$

$$\begin{aligned} m(K)\frac{u_K^{n+1}-u_K^n}{\tau^{n,i}} + \sum_{L\in\mathcal{N}(K)} \tau_{K,L}\left(\varphi_K^{n+1}-\varphi_L^{n+1}\right) \\ + \sum_{\sigma\in\mathcal{F}_{K,\Gamma}^i} \tau_{K,\sigma}\left(\varphi_K^{n+1}-\varphi_{K,\sigma}^{n+1}\right) = 0, \;\; \forall K \in \mathcal{T}_i, \end{aligned} \tag{5.3b}$$

$$-\tau_{K,\sigma}(\varphi_K^{n+1}-\varphi_{K,\sigma}^{n+1}) + \alpha_{ij,\sigma}\Pi_{K,\sigma}^{n+1} = \xi_{\sigma,i}^{n+1}, \;\; \forall \sigma = K|L \in \mathcal{F}_{K,\Gamma}^i \; (K\in\mathcal{T}_i, \; L\in\mathcal{T}_j), \tag{5.3c}$$

where $\xi_{\sigma,i}^{n+1} := \xi_{h\tau,i}(\cdot,t^{n+1})|_\sigma$, $\varphi_K^{n+1} := \varphi(u_K^{n+1})$, $\varphi_{K,\sigma}^{n+1} := \varphi(u_\sigma^{n+1})$, $\Pi_{K,\sigma}^{n+1} = \Pi(u_\sigma^{n+1})$, $\sigma \in \mathcal{F}_{K,\Gamma}^i$, and where we have set $\alpha_{ij,\sigma} = \alpha_{ij\,|\sigma}$.

Then the finite volume approximation of the space–time interface problem (3.4) reads:
find $(\xi_{h\tau,1}, \xi_{h\tau,2}) \in L_{\mathcal{M}_1,h}(\Gamma) \times L_{\mathcal{M}_2,h}(\Gamma)$ such that

$$\begin{aligned} \xi_{h\tau,1} &= \mathcal{P}_{1,2}\mathcal{S}_{2,h}(\xi_{h\tau,2}), \\ \xi_{h\tau,2} &= \mathcal{P}_{2,1}\mathcal{S}_{1,h}(\xi_{h\tau,1}), \end{aligned} \quad \text{on } \Gamma\times(0,T). \tag{5.4}$$

5.3. Convergence result for conforming time discretizations

In this part the time grids are assumed to be conforming: $\mathcal{M} = \mathcal{M}_1 = \mathcal{M}_2$ and we set $M := M_1 = M_2$, $\tau^n := \tau^{n,1} = \tau^{n,2}$, $J^n := J_1^n = J_n^2$, for all $n \in [\![1, M]\!]$. Then problem (5.4) reduces to

$$\begin{aligned} \xi_{h\tau,1} &= \mathcal{S}_{2,h}(\xi_{h\tau,2}), \\ \xi_{h\tau,2} &= \mathcal{S}_{1,h}(\xi_{h\tau,1}), \end{aligned} \quad \text{on } \Gamma\times(0,T). \tag{5.5}$$

We show below that this discrete problem is equivalent to solving local problems, together with natural transmission conditions on Γ: for all $\sigma \in \mathcal{F}_h^\Gamma$, and $\sigma = K|L$, for $K \in \mathcal{T}_{h,1}$, $L \in \mathcal{T}_{h,2}$, for all $n \in [\![0, M-1]\!]$,

$$-\tau_{K,\sigma}\left(\varphi_K^{n+1}-\varphi_{K,\sigma}^{n+1}\right) = \tau_{L,\sigma}\left(\varphi_L^{n+1}-\varphi_{L,\sigma}^{n+1}\right), \tag{5.6a}$$

$$\Pi_{K,\sigma}^{n+1} = \Pi_{L,\sigma}^{n+1}. \tag{5.6b}$$

Lemma 5.1. *Let $\mathcal{D}$ be an admissible discretization of $\Omega\times(0,T)$ in the sense of Definition 5.1. Then the discrete scheme (5.5) is equivalent to the scheme defined by (5.3a)–(5.3b) together with the transmission conditions (5.6a)–(5.6a).*

Proof. The discrete problem (5.5) is equivalent to the solution of the local problems (5.3a)–(5.3c), for $i = 1, 2$, together with the transmission conditions, for $i = 1, 2$, $j = 3-i$,

$$\xi_{h\tau,i} = -\xi_{h\tau,j} + (\alpha_{ji}+\alpha_{ij})\Pi_j(u_{\mathcal{D}_j}), \tag{5.7}$$

or equivalently, for all $\sigma = K|L \in \mathcal{F}_{K,\Gamma}^i$ $(K\in\mathcal{T}_i, \; L\in\mathcal{T}_j)$, for all $n \in [\![1, M_i]\!]$,

$$-\tau_{K,\sigma}(\varphi_K^{n+1}-\varphi_{K,\sigma}^{n+1}) + \alpha_{ij,\sigma}\Pi_{K,\sigma}^{n+1} = \frac{1}{\tau^n}\int_{J^n}\left(\tau_{L,\sigma}(\varphi_L(t)-\varphi_{L,\sigma}(t)) + \alpha_{ij,\sigma}\Pi_{L,\sigma}(t)\right)dt, \tag{5.8}$$

where for a function $\psi \in \mathcal{X}(\mathcal{D})$, $\psi(t) := \psi_K^n$, for $t \in J^n$, and $K \in \mathcal{T}_h$. As stated in Remark 4.3, a function like φ_L belongs to the space $P^0_{\mathcal{M}}(\mathbb{P}_0(\mathcal{F}_h))$, so is constant (in time) on J^n. Thus Eq. (5.8) reduces to the more usual form:

$$-\tau_{K,\sigma}(\varphi_K^{n+1} - \varphi_{K,\sigma}^{n+1}) + \alpha_{ij,\sigma}\Pi_{K,\sigma}^{n+1} = -\tau_{L,\sigma}(\varphi_L^{n+1} - \varphi_{L,\sigma}^{n+1}) + \alpha_{ij,\sigma}\Pi_{L,\sigma}^{n+1}.$$

The two transmission conditions above are easily seen to be algebraically equivalent to (5.6a)–(5.6b). □

Now, the scheme formed by (5.3a)–(5.3b) and (5.6a)–(5.6b) is identical to the multidomain scheme studied in [9,28]. Thus, Lemma 5.1 together with Theorem 2.15 in [9] give the following convergence result:

Corollary 5.1. *Assume that Assumptions 2.1 and 4.1 hold. Let $(\mathcal{D}_m)_m$ be a sequence of admissible discretizations of $\Omega\times(0,T)$, and $\mathcal{D}_{m,i} := \mathcal{D}_m|_{\Omega_i}$, $i = 1, 2$; then, for all $m \in \mathbb{N}$, there exists a discrete solution $u_{\mathcal{D}_m} = (u_{\mathcal{D}_{m,1}}, u_{\mathcal{D}_{m,2}}) \in \mathcal{X}(\mathcal{D}_m|_{\Omega_1}) \times \mathcal{X}(\mathcal{D}_m|_{\Omega_2})$ to the scheme (5.3a)–(5.3c) and (5.8).*

Moreover, if $\lim_{m\to\infty} \mathrm{size}(\mathcal{D}_m) = 0$, and if there exists $\zeta > 0$ such that $\mathrm{reg}(\mathcal{D}_m) \le \zeta$, then, there exists $u \in L^p(\Omega \times (0,T))$, such that (up to a subsequence)

$$u_{\mathcal{D}_m} \to u \in L^p(\Omega \times (0,T)), \quad \forall p \in [1,\infty), \tag{5.9}$$

where u is a weak solution to the multidomain problem (2.6a) to (2.7b) in the sense of Definition 2.1.

5.4. Discrete OSWR algorithm

We now come back to the general case of non-matching time grids. The solution of space–time interface problem (5.4) will be computed by the discrete counterpart of the OSWR algorithm (with possibly non–conforming time grids) described below.

Given an initial iterate $(\xi^0_{h\tau,i})_{i=1,2} \in L_{\mathcal{M}_1,h}(\Gamma)\times L_{\mathcal{M}_2,h}(\Gamma)$, at iteration $k \ge 1$, we calculate in each subdomain Ω_i, $i = 1, 2$, a function $u^k_{\mathcal{D}_i} \in \mathcal{X}(\mathcal{D}_i)$, with $u^k_{\mathcal{D}_i}(\cdot, t^n) := \left((u_K^{k,n})_{K\in\mathcal{T}_i}, (u_\sigma^{k,n})_{\sigma\in\mathcal{F}^i_\Gamma}\right)$, $n \in [\![1, M_i]\!]$, solution of the following discrete subdomain problem with Robin boundary data $\xi^k_{h\tau,i}$: for $n \in [\![0, M_i - 1]\!]$,

$$u_K^{k,0} = \frac{1}{m(K)}\int_K u_0\,\mathrm{d}\mathbf{x}, \ \forall K \in \mathcal{T}_i, \tag{5.10a}$$

$$m(K)\frac{u_K^{k,n+1} - u_K^{k,n}}{\tau^{n,i}} + \sum_{L\in\mathcal{N}(K)} \tau_{K,L}\left(\varphi_K^{k,n+1} - \varphi_L^{k,n+1}\right) + \sum_{\sigma\in\mathcal{F}^i_{K,\Gamma}} \tau_{K,\sigma}\left(\varphi_K^{k,n+1} - \varphi_{K,\sigma}^{k,n+1}\right) = 0, \ \forall K \in \mathcal{T}_i, \tag{5.10b}$$

$$-\tau_{K,\sigma}(\varphi_K^{k,n+1} - \varphi_{K,\sigma}^{k,n+1}) + \alpha_{ij,\sigma}\Pi_{K,\sigma}^{k,n+1} = \xi_{\sigma,i}^{k-1,n+1}, \ \forall \sigma = K|L \in \mathcal{F}^i_{K,\Gamma}\ (K \in \mathcal{T}_i,\ L \in \mathcal{T}_j), \tag{5.10c}$$

where $\xi_{\sigma,i}^{k-1,n+1} := \xi_{h\tau,i}^{k-1}(\cdot, t^{n+1})|_\sigma$, $\varphi_K^{k,n+1} := \varphi(u_K^{k,n+1})$, $\varphi_{K,\sigma}^{k,n+1} := \varphi(u_\sigma^{k,n+1})$, $\Pi_{K,\sigma}^{k,n+1} = \Pi(u_\sigma^{k,n+1})$, $\sigma \in \mathcal{F}^i_{K,\Gamma}$, and then update the new iterates by

$$\xi^k_{h\tau,i} = \mathcal{P}_{i,j}\left(-\xi^{k-1}_{h\tau,j} + (\alpha_{ji} + \alpha_{ij})\Pi_j(u^k_{\mathcal{D}_j})\right). \tag{5.11}$$

Condition (5.10b)–(5.11) can be written in the equivalent form, for all $\sigma = K|L \in \mathcal{F}^i_{K,\Gamma}$ $(K \in \mathcal{T}_i,\ L \in \mathcal{T}_j)$, for all $n \in [\![1, M_i]\!]$,

$$-\tau_{K,\sigma}(\varphi_K^{k,n+1} - \varphi_{K,\sigma}^{k,n+1}) + \alpha_{ij,\sigma}\Pi_{K,\sigma}^{k,n+1} = \frac{1}{\tau_i^n}\int_{J_i^n} \mathcal{P}_{i,j}\left(\tau_{L,\sigma}(\varphi_L^{k-1}(t) - \varphi_{L,\sigma}^{k-1}(t)) + \alpha_{ij,\sigma}\Pi_{L,\sigma}^{k-1}(t)\right)dt. \tag{5.12}$$

In order to show that the above algorithm is well defined, we need to show that Lemma 4.1 can be applied, in order to eliminate the interface unknowns. This is the content of the next Lemma. We have only been able to prove it under the hypothesis that either the scheme is conforming in time, or the capillary pressure functions satisfy the continuity condition

$$\pi_1(0) = \pi_2(0) \text{ and } \pi_1(1) = \pi_2(1). \tag{5.13}$$

Lemma 5.2. *Assume that either the scheme is conforming in time, or that (5.13) holds. Given an element K with a face on the interface $\sigma \in \mathcal{F}^i_{K,\Gamma} \cap \Gamma$, let $L \subset \Omega_j$ such that $\sigma = K|L$. If $\alpha_{ij,\sigma} > \tau_{L,\sigma}$, there exists a unique $u^{k,n+1}_{K,\sigma} \in [0,1]$ solution of (5.12).*

Proof. Assume first that condition (5.13) holds.

We first show that the quantity inside the parenthesis on the right hand side of (5.12) satisfies the hypotheses of Lemma 4.1. Define the function $f : (a,b) \longmapsto \tau_{L,\sigma}\varphi_j(a) + \Big(\alpha_{ij,\sigma}\Pi_j(b) - \tau_{L,\sigma}\varphi_j(b)\Big)$, so that

$$\tau_{L,\sigma}\Big(\varphi^{k-1,n+1}_L - \varphi^{k-1,n+1}_{L,\sigma}\Big) + \alpha_{ij,\sigma}\Pi^{k-1,n+1}_{L,\sigma} = f(u^{k-1,n+1}_L, u^{k-1,n+1}_{L,\sigma}).$$

It is clear that $(a,b) \in [0,1]^2$, and that f is non-decreasing with respect to a. It remains to study f as a function of b. If (5.13) holds, one can compute the partial derivative

$$\frac{\partial f}{\partial b} = (\alpha_{ij,\sigma} - \tau_{L,\sigma})\lambda(u^{k-1,n+1}_{L,\sigma})\pi'_j(u^{k-1,n+1}_{L.\sigma}),$$

which is positive if $\alpha_{ij,\sigma} > \tau_{L,\sigma}$, because π_j is increasing. Thus

$$0 = f(0,0) \le f(u^{k-1,n+1}_L, u^{k-1,n+1}_{L,\sigma}) \le f(1,1) = \alpha_{i,j}\Pi^{k-1,n+1}_{i,\sigma},$$

and the upper bound is actually equal to $\alpha_{ij}\Pi_j(1)$, again because π_1 and π_2 coincide at 0 and 1.

We conclude that the values on the right hand side of (5.12) also satisfy this inequality, as both the projection $\mathcal{P}_{ij}$ and integration preserve monotonicity.

The proof for the case where the scheme is conforming in time uses the equivalent formulation for $\xi_{\tau h,i}$ coming from (5.2) (see also (5.7)). In this case the integral in (5.12) is not needed. We omit the details for the sake of brevity. □

Remark 5.1. The reason we cannot dispense with hypothesis (5.13) is that without it, the functions $\bar{\pi}_i$ and π_i are different, and the partial derivative $\dfrac{\partial f}{\partial b}$ can no longer be computed as in the proof (see the definition of ϕ and Π_i in Section 2.2).

Corollary 5.2 (*Well-posedness of the Algorithm*)**.** *Assume that the scheme is conforming in time or that condition (5.13) holds. Given an initial guess $(\xi^0_{h\tau,i})_{i=1,2} \in L_{\mathcal{M}_1,h}(\Gamma) \times L_{\mathcal{M}_2,h}(\Gamma)$, satisfying Assumption 4.1, and an initial data $u^0_{\mathcal{T}} \in [0,1]$, problem (5.10a) to (5.10b) admits a unique solution $u^k_{\mathcal{D}}$ that satisfies, $\forall 1 \le i \le I$, for all $K \in \mathcal{T}_{h,i}$, for all $n \in [\![1, M_i]\!]$,*

$$0 \le u^{k,n}_K \le 1. \tag{5.14}$$

Proof. The proof is by induction on k. For both the base case $k = 0$ and the induction step, we apply Proposition 4.2. For $k = 0$, $(\xi^0_{h\tau,i})_{i=1,2}$ is assumed to satisfy Assumption 4.1, while for the induction step, this is ensured by Lemma 5.2. □

Remark 5.2. It is possible to improve the robustness of the iterative method and its convergence by replacing the above iterative solver by a more general non-linear solver where problem (5.4) is solved by a Newton-like method.

Remark 5.3. For long time calculations, one could split the time interval into time windows, and in each time window, apply the above domain decomposition method with nonconforming time stepping (cf. [59,63]). Time windows are used in order to reduce the number of iterations of the OSWR-algorithm as shown in the numerical results.

6. Numerical results

We now study the numerical behavior of the Optimized Schwarz waveform relaxation algorithm. For simplicity, we consider constant time steps locally in the subdomains, and define $\tau_i := \tau^{n,i}$, $\forall n \in [\![1, M_i]\!]$, for $i = 1, 2$.

All the results presented were obtained with the help of the Matlab Reservoir Simulation Toolbox[2] [93].

[2] https://www.sintef.no/projectweb/mrst/.

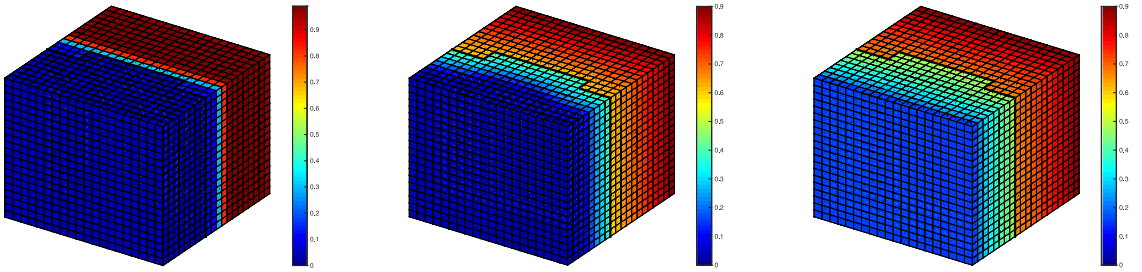

Fig. 6.1. Example 1: saturation $u(t)$, for $t = 0.019$, $t = 0.3$ and $t = 3$.

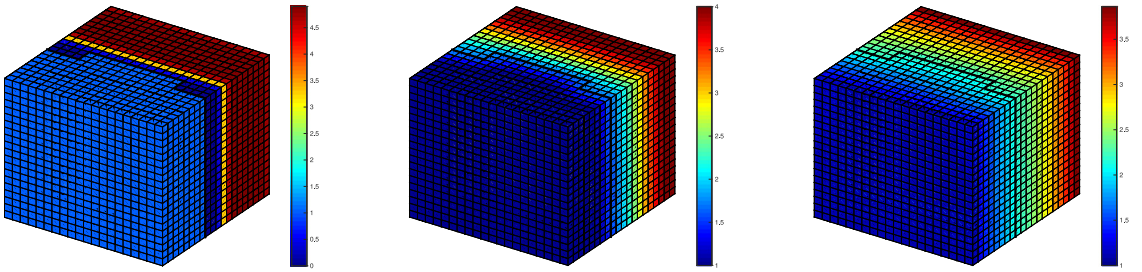

Fig. 6.2. Example 1: Capillary pressure $\pi(u(t))$, for $t = 0.019$, $t = 0.3$ and $t = 3$.

6.1. Example 1: Validation experiment with two rock types

Let us consider a domain $\Omega = [0, 1]^3$ decomposed into two subdomains with two rock types (see top left image on Fig. 6.1). The mobilities are given by

$$\lambda_{o,i}(u) = u, \quad \text{and} \quad \lambda_{g,i}(u) = (1 - u),\ i \in \{1, 2\},$$

and the capillary pressure curves are given by

$$\pi_1(u) = 5u^2, \quad \text{and} \quad \pi_2(u) = 5u^2 + 1.$$

For the initial condition, we suppose that the domain contains some quantity of gas, situated only within Ω_1, i.e.

$$u_0 = \begin{cases} 0.9 & \text{if } x < 0.4, \\ 0 & \text{otherwise.} \end{cases}$$

For the spatial discretization, we use a uniform rectangular mesh with $20 \times 20 \times 20$ elements. For the time discretization, we use nonconforming time grids, constant in each subdomain, with $\tau_1 = 10^{-3}$ and $\tau_2 = \frac{1}{8}10^{-2}$.

The evolution of the saturation at three time steps is shown in Fig. 6.1. We remark that at the beginning of the simulation, approximately until $t \approx 0.02$, the gas cannot penetrate to the domain Ω_2, since the capillary pressure is lower than the threshold value $\pi_2(0) = 1$, which is known as the entry pressure (see Fig. 2.1). The saturation of the trapped gas in Ω_1 as well as the capillary pressure increase until the capillary pressure reaches the entry pressure. This is physically the phenomenon of capillary trapping that model (2.1) describes and which is mathematically due to the degenerate (vanishing) diffusion: indeed, if diffusion was non-vanishing, the gas saturation would be non-zero in the subdomain Ω_2 from the very beginning, and not only after the barrier brake (in contrast to what can be observed in Fig. 6.1).

Fig. 6.2 shows the evolution of the capillary pressure at three time steps. Fig. 6.3 (top) shows evolution of the saturation, the capillary pressure and the diffusion function φ, along a line orthogonal to the interface Γ. We see that the capillary pressure becomes continuous when the entry pressure is reached, and the domain Ω_2 is infiltrated whereas the discontinuity of the saturation and the function φ persists at the interface between the two rocks.

We now analyze the efficiency in time of the method with nonconforming time steps. We compute a reference solution as the converged multidomain solution with conforming fine time grids $\tau_f = \frac{1}{4}10^{-3}$, and where the relative

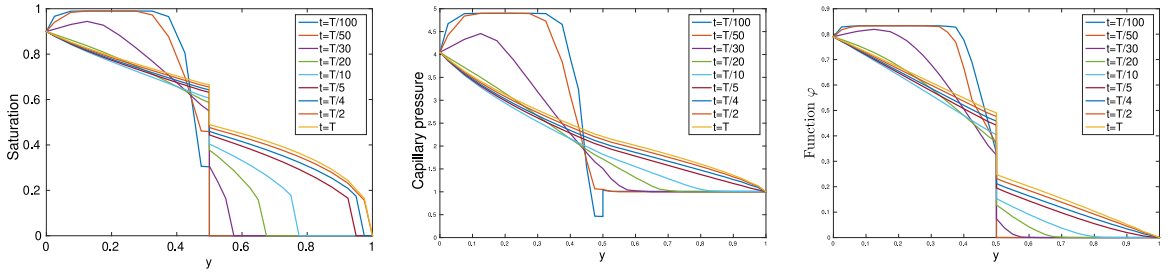

Fig. 6.3. Example 1. From left to right: evolution of the saturation, capillary pressure and diffusion function along a line orthogonal to the interface.

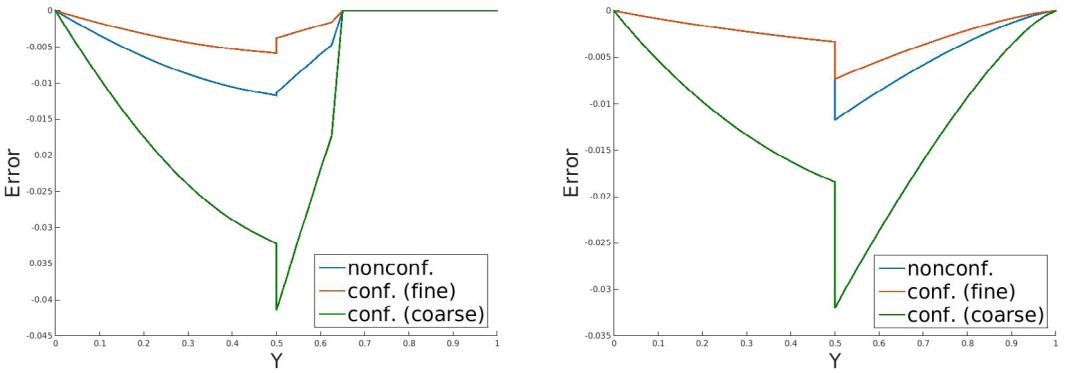

Fig. 6.4. Example 1. Error in saturation along a line orthogonal to the interface, nonconforming and conforming (coarse and fine) time-steps. Left $T = T_f/20$, right, $T = T_f$.

residual is taken smaller than 10^{-12}. We then compare the solution obtained with the nonconforming time steps, as described above with two solutions computed first with conforming fine time steps ($\tau_1 = \tau_2 = 10^{-3}$) and then with conforming coarse time steps (($\tau_1 = \tau_2 = \frac{1}{8}10^{-2}$)). Fig. 6.4 (bottom) shows the error in the saturation along a line orthogonal to the interface at three different time steps. One can see that the nonconforming solution as well as the solution with conforming and fine steps are in close agreement with the reference solution, whereas the solution with coarse time steps has a larger error. This confirms that nonconforming time grids with respect to the rock type preserve the accuracy in time of the multidomain solution.

Finally, we study the convergence behavior of the optimized Schwarz waveform relaxation (OSWR) algorithm. We use as solver for the nonlinear subdomain problems a Newton's method where the tolerance is fixed to 10^{-8}. The tolerance of the OSWR algorithm is 10^{-6}.

Fig. 6.5 shows how the convergence of the OSWR algorithm depends on the value of the optimized transmission parameters α_1 and α_2 (cf. (3.6), but note that to simplify the notation, we let here $\alpha_1 = \alpha_{12}$ and $\alpha_2 = \alpha_{21}$). The left figure shows level curves of the convergence rate as a function of α_1 and α_2. The curves have been computed by running the algorithm for a fixed number of iterations, and noting the residual reached at that stage. The black cross marks the lowest residual, and the red cross marks the values of the parameters obtained by the procedure described at the end of Section 3.2. It is seen that the two values are quite close. Fig. 6.5, right, compares the convergence actually obtained with the two different choices of the optimized parameters, and it can be observed that the convergence for the optimized parameters ($\alpha_1 = 0.13$, $\alpha_2 = 0.15$) is almost as good as that for the observed optimal parameters ($\alpha_1 = 0.18$, $\alpha_2 = 0.15$).

6.2. Example 2: DNAPL infiltration

In this example, we consider a three-dimensional DNAPL infiltration problem with two different rock types. The medium contains a lens with different capillary pressure and relative permeability curves. The gas and water

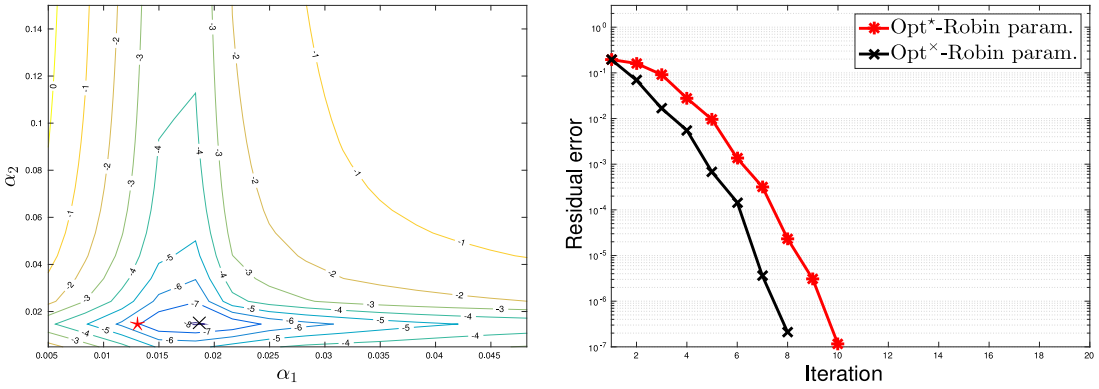

Fig. 6.5. Example 1: Left: Level curves for the residual error obtained after 10 iterations for various values of the parameters α_1 and α_2. The star (in red) marked the parameters obtained with the minimization process of the convergence factor applied to the linearized problem which is close to the best one marked by times symbol (in black). Right: The convergence curves.

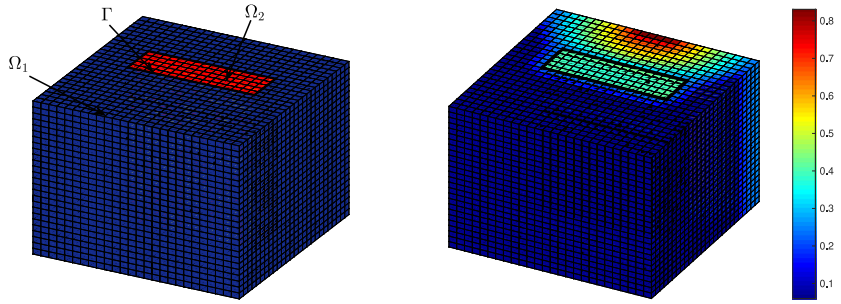

Fig. 6.6. Example 2: Left: geometry and mesh. Right: saturation $u(t)$, for $t = 480$.

mobilities are given by

$$\lambda_{o,i}(u) = u^2, \quad \text{and} \quad \lambda_{g,i}(u) = 3(1-u)^2,\ i \in \{1,2\},$$

and the capillary pressure curves have the form

$$\pi_1(u) = \ln(1-u), \quad \text{and} \quad \pi_2(u) = 0.5 + \ln(1-u).$$

The capillary pressure curves in that case are more complicated as they both go to infinity as u tends to 1. Gas is injected along one side of the domain and a Dirichlet condition is imposed on the opposite face, while no-flow boundary conditions are imposed on the remaining faces.

We use a uniform mesh with 17 576 elements (corresponding to 26 elements in each layer of each direction), and nonconforming time steps with $\tau_1 = 1/2$, and $\tau_2 = 1/3$ for $t \in [0, 500]$. The geometry and the spatial discretization are shown in Fig. 6.6 (left).

Fig. 6.6 (right) shows the saturation over the whole domain at $t = 480$, while Fig. 6.7 shows the saturation on the slice at the middle of the domain Ω in the z-direction (using the same color scale). In this experiment, the flow is driven by the difference in capillary pressure. In contrast to the previous example, when the gas reaches the interface, the flow crosses immediately the interface through the domain Ω_2 and the saturation front snakes along the interface. The gas accumulates into the lens until it eventually spreads into the surrounding medium. The lens acts as a capillary trap (see also [32] or [8]): it is much easier for the gas to enter the lens than to leave it, because of the difference in capillary pressure.

The Robin parameters are again calculated using the procedure of Section 3.2. In Fig. 6.8, we compare the optimized Schwarz method with only one optimized parameter for both subdomains, i.e. $\alpha_{ij} = \alpha_{ji}$ (one-sided method) and that with two different optimized parameters, i.e. $\alpha_{ij} \neq \alpha_{ji}$ (two-sided method). For linear problems, the two-sided method leads to a faster convergence, and its convergence rate is asymptotically much better, see

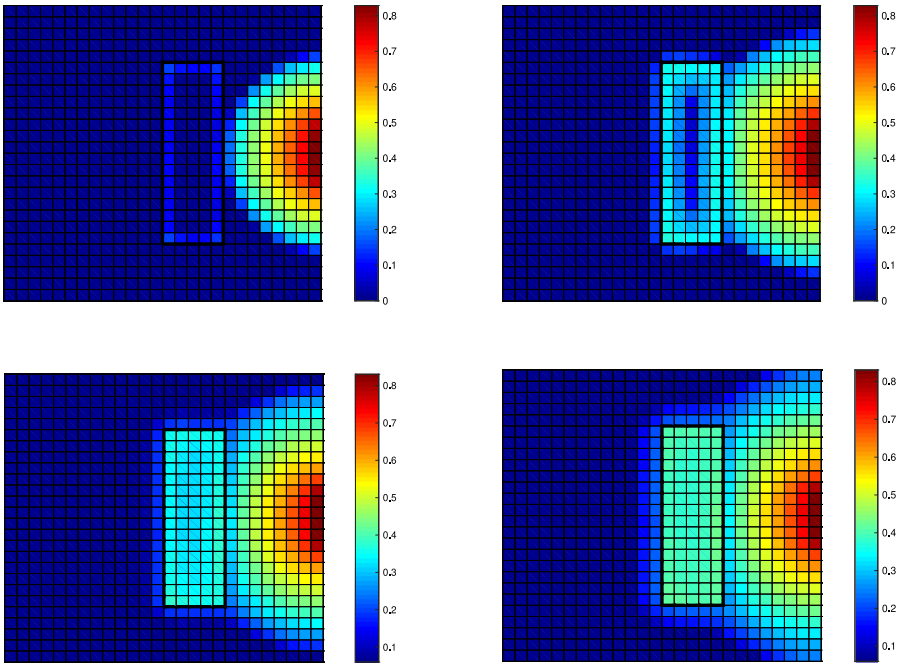

Fig. 6.7. Example 2: Saturation $u(t)$ on a slice at the middle of the domain Ω in the z-direction, for $t = 100$, $t = 200$, $t = 350$, $t = 480$.

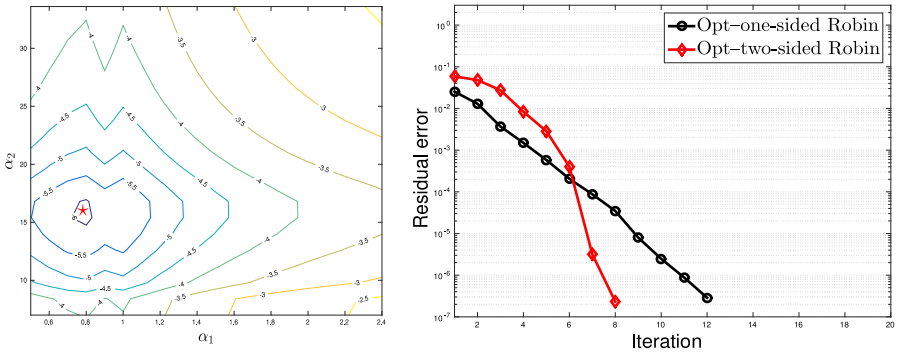

Fig. 6.8. Example 2: Left: Level curves for the residual error obtained after 8 iterations for various values of the parameters α_1 and α_2. The red star shows the optimized parameters. Right: The convergence curves of the optimized Schwarz method with one-sided optimized Robin conditions and two-sided optimized Robin conditions.

e.g. [53]. Here we observe that the two-sided method improves the convergence speed compared to the one-sided method as in the linear case. The two-sided OSWR method needs only 8 iterations to reach a residual error of 10^{-6} compared to the one-sided, which needs 12 iterations.

6.3. Example 3: An example of multidomain solution with time windows for three rock types

Our final example has three rock types as depicted in Fig. 6.9 (left). We use a uniform mesh with 8000 elements, and nonconforming time steps. The mobilities used in this example are the same as in the first example and the capillary pressure curves are given by

$$\pi_1(u) = 3u^2, \quad \pi_2(u) = 5u^2, \text{ and } \quad \pi_3(u) = 3u^2 + 0.5.$$

This numerical experiment shows the ability of the method to satisfy the interface conditions between the different rock types for a more complex geometry. Dirichlet boundary conditions are imposed on the inflow and outflow

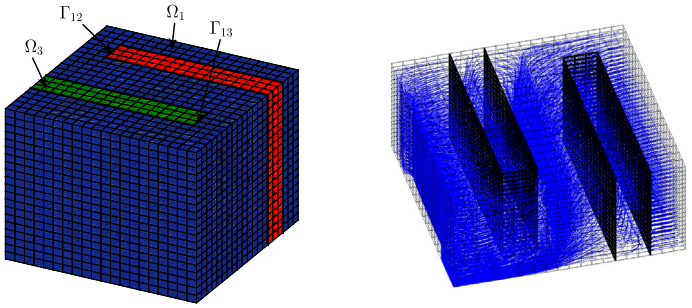

Fig. 6.9. Example 3: Left: The geometry and the mesh. Right: Velocity streamlines.

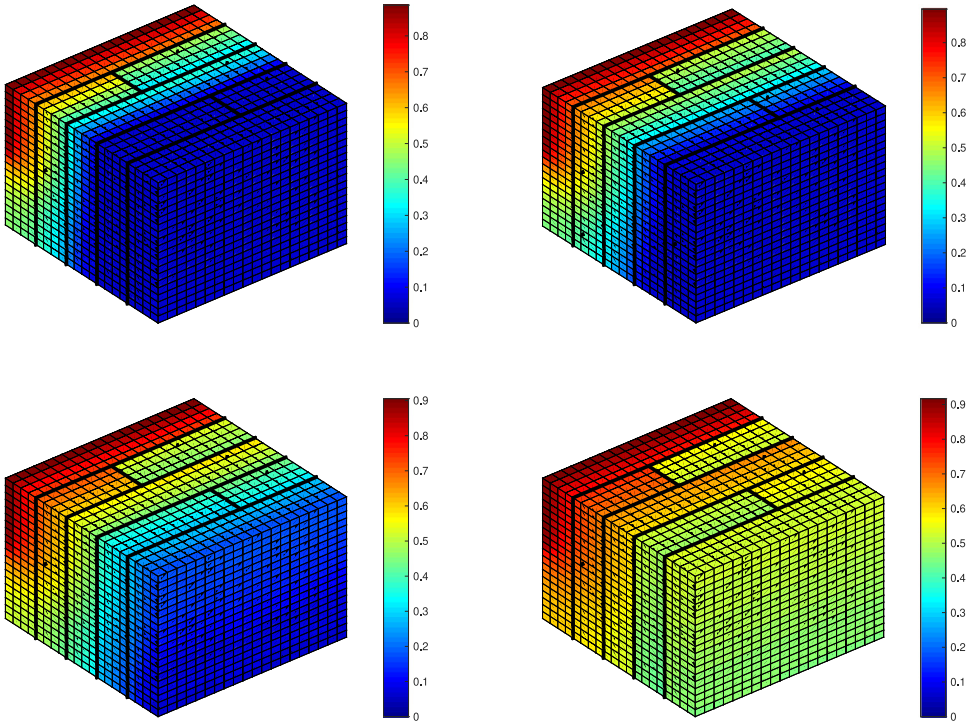

Fig. 6.10. Example 3: Saturation $u(t)$, for $t = 500$, $t = 1000$, $t = 2000$ and $t = 4000$.

boundaries. The inflow boundary, given by $\Gamma_{in} = \{x = 0\} \times \{z > 0.5\}$ has $s = 0.9$. On the outflow boundary $\Gamma_{out} = \{x = 1\}$, the saturation at time t^{n+1} is set equal to that inside the closest cell at time t^n (see [94]).

The space domain is split into 7 subdomains that respect to the rock type (see Fig. 6.10). The spatial grids on the interface are conforming, but the time steps are different in the various subdomains. It was observed that the algorithm converges too slowly to be practical when it is applied over the whole time interval [0, 2500]. Accordingly, the time interval is decomposed into 10 equal *time windows* [59,63]. The OSWR algorithm is employed over one time window at a time, and only after convergence on the current time window is the next time window treated by the algorithm.

The OSWR method needs five iterations to converge in the first time window, and then three iterations for the remaining ones, giving 32 overall. The fact that breaking the interval into time windows allows the OSWR to converge is most likely due a better estimate of the Robin initial guess on the interface afforded by the shorter time intervals.

Fig. 6.10 shows the saturation in the whole domain at four time steps and Fig. 6.9 (right) shows the velocity streamlines in the whole domain. One can see that most of the gas flows through the subdomains Ω_1 that has the

lowest capillary pressure curve. The gas only enters the other subdomains once the capillary pressure reaches the entry pressure for the respective rock.

7. Conclusion

This paper combines an Optimized Schwarz Waveform Relaxation method with a finite volume scheme for the discretization of two-phase flows in a porous medium made up of different rock types. The model problem we consider only takes into account the diffusive effects for the saturation, and deals with discontinuous capillary pressure curves at the interface between the rocks. An existence result for the subdomain two-phase flow problem with nonlinear Robin boundary condition is presented.

The OSWR algorithm provides a natural way to treat the discontinuity of the saturation between rock types. The method allows for different time steps in the subdomains, so as to adapt to the time scales imposed by the different capillary pressure curves. A discontinuous Galerkin method in time is used, with projection between the space–time grids on the interfaces to match the local solutions. The convergence of the scheme is improved through the use of time windows. Several numerical results confirm that the nonlinear interface conditions, which are enforced in the context of a OSWR-algorithm, are captured in a robust and accurate way.

Further work is currently under way to extend the present work to handle the full two–phase flow case.

Declaration of competing interest

The authors declare that they have no known competing financial interests or personal relationships that could have appeared to influence the work reported in this paper.

Acknowledgments

The authors warmly thank Clément Cancès and Robert Eymard for enlightening discussions that helped us to carry out the proof of Theorem 4.1.

References

[1] B. Amaziane, M. El Ossmani, M. Jurak, Numerical simulation of gas migration through engineered and geological barriers for a deep repository for radioactive waste, Comput. Vis. Sci. 15 (1) (2012) 3–20, http://dx.doi.org/10.1007/s00791-013-0196-1.

[2] Z. Acem, J. Lopez, E.P.D. Barrio, KNO3/NaNO3 – Graphite materials for thermal energy storage at high temperature: Part I. – Elaboration methods and thermal properties, Appl. Therm. Eng. 30 (13) (2010) 1580–1585, http://dx.doi.org/10.1016/j.applthermaleng.2010.03.013.

[3] B.S. Zhilin Li, Fast and accurate numerical approaches for Stefan problems and cystal growth, Numer. Heat Transfer B 35 (4) (1999) 461–484, http://dx.doi.org/10.1080/104077999275848, arXiv:https://doi.org/10.1080/104077999275848.

[4] B. Amaziane, S. Antontsev, L. Pankratov, A. Piatnitski, Homogenization of immiscible compressible two-phase flow in porous media: application to gas migration in a nuclear waste repository, Multiscale Model. Simul. 8 (5) (2010) 2023–2047.

[5] B. Amaziane, M. El Ossmani, M. Jurak, Numerical simulation of gas migration through engineered and geological barriers for a deep repository for radioactive waste, Comput. Vis. Sci. 15 (1) (2012) 3–20.

[6] A. Bourgeat, M. Jurak, A two level scaling-up method for multiphase flow in porous media; numerical validation and comparison with other methods, Comput. Geosci. 14 (1) (2010) 1–14, http://dx.doi.org/10.1007/s10596-009-9128-z.

[7] C.J. Van Duijn, J. Molenaar, M.J. De Neef, The effect of capillary forces on immiscible two-phase flow in heterogeneous porous media, Transp. Porous Media 21 (1) (1995) 71–93, http://dx.doi.org/10.1007/BF00615335.

[8] M. Bertsch, R. Dal Passo, C. Van Duijn, Analysis of oil trapping in porous media flow, SIAM J. Math. Anal. 35 (1) (2003) 245–267.

[9] G. Enchéry, R. Eymard, A. Michel, Numerical approximation of a two-phase flow problem in a porous medium with discontinuous capillary forces, SIAM J. Numer. Anal. 43 (6) (2006) 2402–2422, http://dx.doi.org/10.1137/040602936.

[10] H.W. Alt, S. Luckhaus, Quasilinear elliptic-parabolic differential equations, Math. Z. 183 (3) (1983) 311–341, http://dx.doi.org/10.1007/BF01176474.

[11] R. Eymard, T. Gallouët, D. Hilhorst, Y. Naït Slimane, Finite volumes and nonlinear diffusion equations, RAIRO-Modél. Math. Anal. Numér. 32 (6) (1998) 747–761.

[12] R. Eymard, T. Gallouët, R. Herbin, Finite volume methods, in: P.G. Ciarlet, J.-L. Lions (Eds.), Handbook of Numerical Analysis, Vol. 7, Elsevier, 2000, pp. 713–1018.

[13] R. Eymard, C. Guichard, R. Herbin, R. Masson, Gradient schemes for two-phase flow in heterogeneous porous media and Richards equation, ZAMM Z. Angew. Math. Mech. 94 (7–8) (2014) 560–585, http://dx.doi.org/10.1002/zamm.201200206.

[14] J. Droniou, R. Eymard, T. Gallouët, C. Guichard, R. Herbin, The Gradient Discretisation Method, in: Mathématiques & Applications (Berlin), vol. 82, Springer, Cham, 2018, p. xxiv+497.

[15] F. List, K. Kumar, I.S. Pop, F.A. Radu, Rigorous upscaling of unsaturated flow in fractured porous media, SIAM J. Math. Anal. 52 (1) (2020) 239–276, http://dx.doi.org/10.1137/18M1203754.
[16] X. Cao, I.S. Pop, Uniqueness of weak solutions for a pseudo-parabolic equation modeling two phase flow in porous media, Appl. Math. Lett. 46 (2015) 25–30, http://dx.doi.org/10.1016/j.aml.2015.01.022.
[17] F.A. Radu, I.S. Pop, P. Knabner, Error estimates for a mixed finite element discretization of some degenerate parabolic equations, Numer. Math. 109 (2) (2008) 285–311, http://dx.doi.org/10.1007/s00211-008-0139-9.
[18] F.A. Radu, K. Kumar, J.M. Nordbotten, I.S. Pop, A robust, mass conservative scheme for two-phase flow in porous media including Hölder continuous nonlinearities, IMA J. Numer. Anal. 38 (2) (2018) 884–920, http://dx.doi.org/10.1093/imanum/drx032.
[19] G. Chavent, J. Jaffré, Mathematical Models and Finite Elements for Reservoir Simulation: Single Phase, Multiphase and Multicomponent Flows through Porous Media, Elsevier, 1986.
[20] Z. Chen, R.E. Ewing, Degenerate two-phase incompressible flow. IV. Local refinement and domain decomposition, J. Sci. Comput. 18 (3) (2003) 329–360, http://dx.doi.org/10.1023/A:1022673427893.
[21] Z. Chen, Degenerate two-phase incompressible flow. I. Existence, uniqueness and regularity of a weak solution, J. Differential Equations 171 (2) (2001) 203–232, http://dx.doi.org/10.1006/jdeq.2000.3848.
[22] T. Arbogast, The existence of weak solutions to single porosity and simple dual-porosity models of two-phase incompressible flow, Nonlinear Anal. TMA 19 (11) (1992) 1009–1031, http://dx.doi.org/10.1016/0362-546X(92)90121-T.
[23] Z. Chen, R. Ewing, Mathematical analysis for reservoir models, SIAM J. Math. Anal. 30 (2) (1999) 431–453, http://dx.doi.org/10.1137/S0036141097319152.
[24] B. Schweizer, Homogenization of degenerate two-phase flow equations with oil trapping, SIAM J. Math. Anal. 39 (6) (2008) 1740–1763, http://dx.doi.org/10.1137/060675472.
[25] B. Amaziane, A. Bourgeat, H. El Amri, Existence of solutions to various rock types model of two-phase flow in porous media, Appl. Anal. 60 (1–2) (1996) 121–132, http://dx.doi.org/10.1080/00036819608840421.
[26] W. Jäger, L. Simon, On transmission problems for nonlinear parabolic differential equations, Ann. Univ. Sci. Budapest. Eötvös Sect. Math. 45 (2002) 143–158, (2003).
[27] L. Simon, On contact problems for nonlinear parabolic functional differential equations, in: Proceedings of the 7th Colloquium on the Qualitative Theory of Differential Equations, Vol. 7, Electron. J. Qual. Theory Differ. Equ., Szeged, 2004, pp. No. 22, 11.
[28] C. Cancès, Nonlinear parabolic equations with spatial discontinuities, NoDEA Nonlinear Differential Equations Appl. 15 (4–5) (2008) 427–456, http://dx.doi.org/10.1007/s00030-008-6030-7.
[29] C. Cancès, On the effects of discontinuous capillarities for immiscible two-phase flows in porous media made of several rock-types, NHM 5 (3) (2010) 635–647.
[30] C. Cancès, Finite volume scheme for two-phase flows in heterogeneous porous media involving capillary pressure discontinuities, M2AN Math. Model. Numer. Anal. 43 (5) (2009) 973–1001, http://dx.doi.org/10.1051/m2an/2009032.
[31] K. Brenner, C. Cancès, D. Hilhorst, Finite volume approximation for an immiscible two-phase flow in porous media with discontinuous capillary pressure, Comput. Geosci. 17 (3) (2013) 573–597, http://dx.doi.org/10.1007/s10596-013-9345-3.
[32] A. Ern, I. Mozolevski, L. Schuh, Discontinuous Galerkin approximation of two-phase flows in heterogeneous porous media with discontinuous capillary pressures, Comput. Methods Appl. Mech. Engrg. 199 (23–24) (2010) 1491–1501, http://dx.doi.org/10.1016/j.cma.2009.12.014.
[33] P. Henning, M. Ohlberger, B. Schweizer, Adaptive heterogeneous multiscale methods for immiscible two-phase flow in porous media, Comput. Geosci. 19 (1) (2015) 99–114, http://dx.doi.org/10.1007/s10596-014-9455-6.
[34] C. Cancès, T. Gallouët, A. Porretta, Two-phase flows involving capillary barriers in heterogeneous porous media, Interfaces Free Bound. 11 (2) (2009) 239–258, http://dx.doi.org/10.4171/IFB/210.
[35] I. Yotov, A mixed finite element discretization on non-matching multiblock grids for a degenerate parabolic equation arising in porous media flow, East-West J. Numer. Math. 5 (3) (1997) 211–230.
[36] I. Yotov, Interface solvers and preconditioners of domain decomposition type for multiphase flow in multiblock porous media, in: Scientific Computing and Applications, in: Adv. Comput. Theory Pract., vol. 7, Nova Sci. Publ., Huntington, NY, 2001, pp. 157–167.
[37] E. Ahmed, Splitting-based domain decomposition methods for two-phase flow with different rock types, Adv. Water Resour. 134 (2019) 103431, http://dx.doi.org/10.1016/j.advwatres.2019.103431.
[38] B. Ganis, K. Kumar, G. Pencheva, M.F. Wheeler, I. Yotov, A global Jacobian method for mortar discretizations of a fully implicit two-phase flow model, Multiscale Model. Simul. 12 (4) (2014) 1401–1423, http://dx.doi.org/10.1137/140952922.
[39] J.O. Skogestad, E. Keilegavlen, J.M. Nordbotten, Domain decomposition strategies for nonlinear flow problems in porous media, J. Comput. Phys. 234 (2013) 439–451, http://dx.doi.org/10.1016/j.jcp.2012.10.001.
[40] J.O. Skogestad, E. Keilegavlen, J.M. Nordbotten, Two-scale preconditioning for two-phase nonlinear flows in porous media, Transp. Porous Media 114 (2) (2016) 485–503, http://dx.doi.org/10.1007/s11242-015-0587-5.
[41] D. Seus, F.A. Radu, C. Rohde, A linear domain decomposition method for two-phase flow in porous media, in: Numerical Mathematics and Advanced Applications—ENUMATH 2017, in: Lect. Notes Comput. Sci. Eng., vol. 126, Springer, 2019, pp. 603–614, http://dx.doi.org/10.1007/978-3-319-96415-7_55.
[42] D. Seus, K. Mitra, I.S. Pop, F.A. Radu, C. Rohde, A linear domain decomposition method for partially saturated flow in porous media, Comput. Methods Appl. Mech. Engrg. 333 (2018) 331–355, http://dx.doi.org/10.1016/j.cma.2018.01.029.
[43] E. Ahmed, S. Ali Hassan, C. Japhet, M. Kern, M. Vohralík, A posteriori error estimates and stopping criteria for space-time domain decomposition for two-phase flow between different rock types, SMAI J. Comput. Math. 5 (2019) 195–227, http://dx.doi.org/10.5802/smai-jcm.47.
[44] D. Bennequin, M.J. Gander, L. Halpern, A homographic best approximation problem with application to optimized Schwarz waveform relaxation, Math. Comp. 78 (265) (2009) 185–223, http://dx.doi.org/10.1090/S0025-5718-08-02145-5.

[45] T.-P. Hoang, J. Jaffré, C. Japhet, M. Kern, J.E. Roberts, Space-time domain decomposition methods for diffusion problems in mixed formulations, SIAM J. Numer. Anal. 51 (6) (2013) 3532–3559.
[46] H. Berninger, S. Loisel, O. Sander, The 2-Lagrange multiplier method applied to nonlinear transmission problems for the Richards equation in heterogeneous soil with cross points, SIAM J. Sci. Comput. 36 (5) (2014) A2166–A2198, http://dx.doi.org/10.1137/120901064.
[47] F. Haeberlein, L. Halpern, A. Michel, Newton-Schwarz optimised waveform relaxation Krylov accelerators for nonlinear reactive transport, in: Domain Decomposition Methods in Science and Engineering XX, in: Lect. Notes Comput. Sci. Eng., vol. 91, Springer, Heidelberg, 2013, pp. 387–394, http://dx.doi.org/10.1007/978-3-642-35275-1_45.
[48] L. Halpern, F. Hubert, A finite volume Ventcell-Schwarz algorithm for advection-diffusion equations, SIAM J. Numer. Anal. 52 (3) (2014) 1269–1291.
[49] K. Santugini, A discontinuous coarse space (DCS) algorithm for cell centered finite volume based domain decomposition methods: The DCS-RJMin algorithm, in: Domain Decomposition Methods in Science and Engineering XXII, Springer, 2016, pp. 379–387.
[50] P.-L. Lions, On the Schwarz alternating method. III. A variant for nonoverlapping subdomains, in: Third International Symposium on Domain Decomposition Methods for Partial Differential Equations (Houston, TX, 1989), SIAM, Philadelphia, PA, 1990, pp. 202–223.
[51] C. Japhet, F. Nataf, The best interface conditions for domain decomposition methods: absorbing boundary conditions, in: Absorbing Boundaries and Layers, Domain Decomposition Methods, Nova Sci. Publ., Huntington, NY, 2001, pp. 348–373.
[52] V. Martin, An optimized Schwarz waveform relaxation method for the unsteady convection diffusion equation in two dimensions, Appl. Numer. Math. 52 (4) (2005) 401–428, http://dx.doi.org/10.1016/j.apnum.2004.08.022.
[53] M.J. Gander, Optimized Schwarz methods, SIAM J. Numer. Anal. 44 (2) (2006) 699–731, http://dx.doi.org/10.1137/S0036142903425409, (electronic).
[54] T.T.P. Hoang, C. Japhet, M. Kern, J.E. Roberts, Ventcell conditions with mixed formulations for flow in porous media, in: T. Dickopf, M. Gander, L. Halpern, R. Krause, L.F. Pavarino (Eds.), Domain Decomposition Methods in Science and Engineering XXII, in: Lecture Notes in Computational Science and Engineering, vol. 104, Springer, 2016, pp. 531–540.
[55] F. Caetano, M.J. Gander, L. Halpern, J. Szeftel, et al., Schwarz waveform relaxation algorithms for semilinear reaction-diffusion equations, NHM 5 (3) (2010) 487–505.
[56] W. Chen, M. Gunzburger, F. Hua, X. Wang, A parallel Robin–Robin domain decomposition method for the Stokes—Darcy system, SIAM J. Numer. Anal. 49 (3) (2011) 1064–1084, http://dx.doi.org/10.1137/080740556.
[57] M. Discacciati, A. Quarteroni, A. Valli, Robin—Robin domain decomposition methods for the Stokes—Darcy coupling, SIAM J. Numer. Anal. 45 (3) (2007) 1246–1268, http://dx.doi.org/10.1137/06065091X.
[58] U. Wilbrandt, Stokes–Darcy Equations: Analytic and Numerical Analysis, Springer International Publishing, Cham, 2019, http://dx.doi.org/10.1007/978-3-030-02904-3_1.
[59] E. Blayo, L. Halpern, C. Japhet, Optimized Schwarz waveform relaxation algorithms with nonconforming time discretization for coupling convection-diffusion problems with discontinuous coefficients, in: Domain Decomposition Methods in Science and Engineering XVI, in: Lect. Notes Comput. Sci. Eng., vol. 55, Springer, Berlin, 2007, pp. 267–274, http://dx.doi.org/10.1007/978-3-540-34469-8_31.
[60] S. Théry, C. Pelletier, F. Lemarié, E. Blayo, Analysis of Schwarz waveform relaxation for the coupled ekman boundary layer problem with continuously variable coefficients, 2020, working paper or preprint. URL https://hal.inria.fr/hal-02544113.
[61] C. Pelletier, Mathematical Study of the Air-Sea Coupling Problem Including Turbulent Scale Effects (Theses), Université Grenoble Alpes, 2018, URL https://tel.archives-ouvertes.fr/tel-01717274.
[62] M. Tayachi Pigeonnat, A. Rousseau, E. Blayo, N. Goutal, V. Martin, Design and analysis of a Schwarz coupling method for a dimensionally heterogeneous problem, Int. J. Numer. Methods Fluids 75 (6) (2014) 446–465, http://dx.doi.org/10.1002/d.3902.
[63] L. Halpern, C. Japhet, J. Szeftel, Optimized Schwarz waveform relaxation and discontinuous Galerkin time stepping for heterogeneous problems, SIAM J. Numer. Anal. 50 (5) (2012) 2588–2611, http://dx.doi.org/10.1137/120865033.
[64] T.-T.-P. Hoang, C. Japhet, M. Kern, J.E. Roberts, Space-time domain decomposition for advection-diffusion problems in mixed formulations, Math. Comput. Simulation 137 (2017) 366–389, http://dx.doi.org/10.1016/j.matcom.2016.11.002.
[65] E. Ahmed, C. Japhet, M. Kern, Global-in-time domain decomposition for a nonlinear diffusion problem, in: 25th International Domain Decomposition Conference, DD25, Springer, St John's, Canada, 2018, (Accepted).
[66] E. Ahmed, C. Japhet, M. Kern, Space-time domain decomposition for two-phase flow between different rock types, 2020, working paper or preprint, hal-02275690 version 2.
[67] C. Cancès, I.S. Pop, M. Vohralík, An a posteriori error estimate for vertex-centered finite volume discretizations of immiscible incompressible two-phase flow, Math. Comp. 83 (285) (2014) 153–188, http://dx.doi.org/10.1090/S0025-5718-2013-02723-8.
[68] M. Vohralík, M.F. Wheeler, A posteriori error estimates, stopping criteria, and adaptivity for two-phase flows, Comput. Geosci. 17 (5) (2013) 789–812, http://dx.doi.org/10.1007/s10596-013-9356-0.
[69] K. Aziz, A. Settari, Petroleum Reservoir Simulation, Applied Science Publishers, 1979.
[70] J.W. Both, K. Kumar, J.M. Nordbotten, I.S. Pop, F.A. Radu, Iterative linearisation schemes for doubly degenerate parabolic equations, in: Numerical Mathematics and Advanced Applications—ENUMATH 2017, in: Lect. Notes Comput. Sci. Eng., vol. 126, Springer, Cham, 2019, pp. 49–63, http://dx.doi.org/10.1007/978-3-319-96415-7_3.
[71] J. Bear, Y. Bachmat, Introduction to Modeling of Transport Phenomena in Porous Media, Vol. 4, Springer Science & Business Media, 2012.
[72] B. Andreianov, K. Brenner, C. Cancès, Approximating the vanishing capillarity limit of two-phase flow in multi-dimensional heterogeneous porous medium, ZAMM Z. Angew. Math. Mech. 94 (7–8) (2014) 655–667, http://dx.doi.org/10.1002/zamm.201200218.
[73] V. Dolean, P. Jolivet, F. Nataf, An Introduction to Domain Decomposition Methods. Algorithms, Theory, and Parallel Implementation, Society for Industrial and Applied Mathematics (SIAM), Philadelphia, PA, 2015, p. x+238, http://dx.doi.org/10.1137/1.9781611974065.ch1.

[74] S. Ali Hassan, C. Japhet, M. Kern, M. Vohralík, A posteriori stopping criteria for optimized Schwarz domain decomposition algorithms in mixed formulations, Comput. Methods Appl. Math. 18 (3) (2018) 495–519, http://dx.doi.org/10.1515/cmam-2018-0010.
[75] S. Ali Hassan, C. Japhet, M. Vohralík, A posteriori stopping criteria for space-time domain decomposition for the heat equation in mixed formulations, Electron. Trans. Numer. Anal. 49 (2018) 151–181, http://dx.doi.org/10.1553/etna_vol49s151.
[76] M.J. Gander, L. Halpern, F. Nataf, Optimal Schwarz waveform relaxation for the one dimensional wave equation, SIAM J. Numer. Anal. 41 (5) (2003) 1643–1681, http://dx.doi.org/10.1137/S003614290139559X.
[77] F. Lemarié, L. Debreu, E. Blayo, Toward an optimized global-in-time Schwarz algorithm for diffusion equations with discontinuous and spatially variable coefficients. Part 2: The variable coefficients case, Electron. Trans. Numer. Anal. 40 (2013) 170–186.
[78] F. Lemarié, L. Debreu, E. Blayo, Toward an optimized global-in-time Schwarz algorithm for diffusion equations with discontinuous and spatially variable coefficients. Part 1: The constant coefficients case, Electron. Trans. Numer. Anal. 40 (2013) 148–169.
[79] M.J. Gander, L. Halpern, Optimized Schwarz waveform relaxation methods for advection reaction diffusion problems, SIAM J. Numer. Anal. 45 (2) (2007) 666–697, http://dx.doi.org/10.1137/050642137.
[80] P.-M. Berthe, C. Japhet, P. Omnes, Space-time domain decomposition with finite volumes for porous media applications, in: J. Erhel, M. Gander, L. Halpern, G. Pichot, T. Sassi, O. Widlund (Eds.), Domain Decomposition Methods in Science and Engineering XXI, in: Lecture Notes in Computational Science and Engineering, vol. 98, 2014, pp. 483–490.
[81] D.A. Di Pietro, E. Flauraud, M. Vohralík, S. Yousef, A posteriori error estimates, stopping criteria, and adaptivity for multiphase compositional Darcy flows in porous media, J. Comput. Phys. 276 (2014) 163–187, http://dx.doi.org/10.1016/j.jcp.2014.06.061.
[82] P.G. Ciarlet, Linear and Nonlinear Functional Analysis with Applications, SIAM, 2013.
[83] J.M. Ortega, W.C. Rheinboldt, Iterative Solution of Nonlinear Equations in Several Variables, in: Computer Science and Applied Mathematics, Academic Press, 1970.
[84] B. Andreianov, C. Cancès, A. Moussa, A nonlinear time compactness result and applications to discretization of degenerate parabolic-elliptic PDEs, J. Funct. Anal. 273 (12) (2017) 3633–3670, http://dx.doi.org/10.1016/j.jfa.2017.08.010.
[85] A. Ait Hammou Oulhaj, Numerical analysis of a finite volume scheme for a seawater intrusion model with cross-diffusion in an unconfined aquifer, Numer. Methods Partial Differential Equations 34 (3) (2018) 857–880, http://dx.doi.org/10.1002/num.22234.
[86] A. Ait Hammou Oulhaj, C. Cancès, C. Chainais-Hillairet, Numerical analysis of a nonlinearly stable and positive control volume finite element scheme for Richards equation with anisotropy, ESAIM: M2AN 52 (4) (2018) 1533–1567, http://dx.doi.org/10.1051/m2an/2017012.
[87] N. Igbida, Hele-shaw type problems with dynamical boundary conditions, J. Math. Anal. Appl. 335 (2) (2007) 1061–1078.
[88] L. Ambrosio, G. Dal Maso, A general chain rule for distributional derivatives, Proc. Amer. Math. Soc. 108 (3) (1990) 691–702, http://dx.doi.org/10.2307/2047789.
[89] R. Eymard, T. Gallouët, R. Herbin, A. Michel, Convergence of a finite volume scheme for nonlinear degenerate parabolic equations, Numer. Math. 92 (1) (2002) 41–82, http://dx.doi.org/10.1007/s002110100342.
[90] B. Andreianov, M.K. Gazibo, Entropy formulation of degenerate parabolic equation with zero-flux boundary condition, Z. Angew. Math. Phys. 64 (5) (2013) 1471–1491.
[91] L. Halpern, C. Japhet, J. Szeftel, Discontinuous Galerkin and nonconforming in time optimized Schwarz waveform relaxation, in: Domain Decomposition Methods in Science and Engineering XIX, Springer, 2011, pp. 133–140.
[92] F. Haeberlein, L. Halpern, A. Michel, Schwarz waveform relaxation and Krylov accelerators for reactive transport, 2015, working paper or preprint.
[93] K.-A. Lie, An Introduction to Reservoir Simulation Using MATLAB/GNU Octave. User Guide for the MATLAB Reservoir Simulation Toolbox (MRST), Cambridge University Press, 2019, http://dx.doi.org/10.1017/9781108591416.
[94] E. Ahmed, J. Jaffré, J.E. Roberts, A reduced fracture model for two-phase flow with different rock types, Math. Comput. Simulation 137 (2017) 49–70, http://dx.doi.org/10.1016/j.matcom.2016.10.005.